# 11. The Finite Integration Technique as a General Tool to Compute Acoustic, Electromagnetic, Elastodynamic, and Coupled Wave Fields

***René Marklein***
University of Kassel, Department of Electrical Engineering/Computer Science,
Electromagnetic Field Theory, Wilhelmhöher Allee 71, D-34121 Kassel, Germany
Tel: +49 (561) 804-6426; Fax: +49 (561) 804-6489; E-mail: marklein@uni-kassel.de
http://www.tet.e-technik.uni-kassel.de; http://www.uni-kassel.de/fb16/tet/marklein

**Dedicated to Professor Dr. K. J. Langenberg on the occasion of his 60th birthday**

## 1. ABSTRACT

This review paper presents a unified treatment of the numerical time-domain modeling of acoustic, electromagnetic, and elastodynamic waves and of the combination thereof: this means coupled wave fields, like piezoelectric (elasto-electric) and electromagnetic-ultrasonic wave fields. Since the famous paper by *Yee* [*1966*], the time-domain solution of Maxwell's equations has become very popular, and this initiated the Finite-Difference Time-Domain (FDTD) Method [*Taflove and Hagness*, *2000*; *fdtd.org*, *2001*]. Ten years later, *Madariaga* [*1976*] independently developed a similar method in elastodynamics. Both methods start from the governing equations in differential form, using standard second-order finite-difference stencils in space and time. In electromagnetics, *Weiland* [*1977*] introduced a different approach, which starts from the full set of Maxwell's equations in integral form. Today, this method is commonly called the Finite Integration Technique (FIT). In the 1990s, based on Weiland's ideas, *Fellinger* [*1991*] adapted the FIT to the elastodynamic case. Today, a toolbox of several modeling codes – called AFIT, EMFIT, EFIT, PFIT, and EMUSFIT, which stand for acoustic (A), electromagnetic (EM), elastic (E), piezoelectric (P), and electromagnetic-ultrasonic (EMUS) Finite Integration Technique (FIT) – is available [*Marklein*, *1997*, *2000a*, *b*]. In all these cases, the underlying governing equations in integral form are discretized with the FIT on a dual grid complex in space and time, which yields the so-called discrete grid equations. One of the advantages of the FIT approach is that the resulting discrete matrix equations represent a consistent one-to-one translation of the underlying field equations. Discrete topological operators are introduced, which ensure important vector analytical properties in the discrete grid space. The FIT implicitly insures that the numerical results are free of late-time instabilities and artificial sources. Simplicity is another important advantage of the FIT, which allows an easy and efficient implementation on various computer architectures. The underlying theory and the derivation of the numerical codes are presented in a unified way. The numerical examples and applications were computed with the software package *fit* [*Marklein*, *1997*, *2000a*, *b*].

## 2. INTRODUCTION

The computational time-domain modeling of different types of wave-field problems is utilized in various disciplines of engineering and science: in increasingly challenging problems in

remote sensing, communications, optics, geophysical exploration, ground-penetrating radar, medical diagnosis, and nondestructive evaluation. Figures 1 and 2 display typical sketches of the setups used in nondestructive testing and material characterization. Figure 3 shows a typical transient echo signal of the setup shown in Figure 2. Various numerical techniques are applied today to model transient wave fields in acoustics, electromagnetics, and elastodynamics, as well as coupled effects thereof: for instance, the Finite-Difference (FD), Finite-Element (FE), Finite-Volume (FV), Finite-Difference Time-Domain (FDTD), Finite-Integration (FI), and Finite-Volume Time-Domain (FVTD) Methods, as well as the recently introduced Microcell Time-Domain (MCTD) Method [*Marrone*, *2001*], which is an extension of the novel cell method proposed by *Tonti* [*2001a*] (see also [*Discrete Physics*, *2001*]). This review paper mainly focuses on the Finite Integration Technique (FIT).

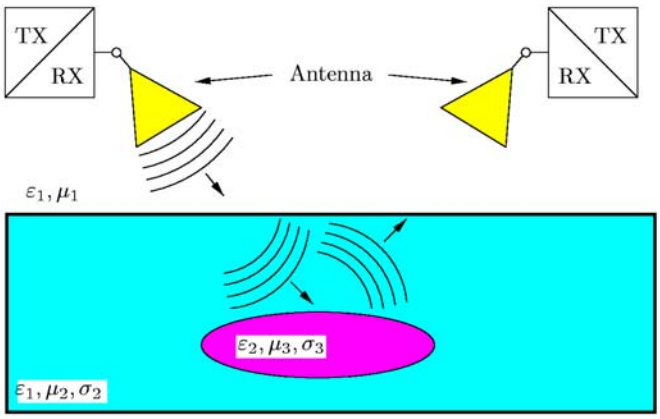


**Figure 1.** A typical measurement setup used in nondestructive testing/material characterization with electromagnetic wave fields: test sample with a penetrable inclusion. TX: transmitter; RX: receiver; $\varepsilon_i$, $\mu_i$, and $\sigma_i$ are the permittivity, permeability, and electric conductivity of the *i*th material.

Historically, *Weiland* [*1977*] introduced the Finite Integration Technique (FIT) three decades ago in electrodynamics, where FIT was applied to the full set of Maxwell's equations in integral form. The method uses all six vector components of electric field strength and magnetic flux density on a dual grid system [*Weiland*, *1986*; *Bartsch et al.*, *1992*]. *Weiland* [*1996*] reformulated the Finite Integration Technique in terms of global quantities assigned to space objects – like the electric and magnetic (grid) voltage assigned to a contour, and the electric and magnetic (grid) flux assigned to a surface – which allows a matrix formulation, also valid for irregular and non-orthogonal grid systems. In a recently published book, *Van Rienen* [*2001a*] presented a detailed description of these ideas (see also [*Thoma*, *1997*; *Clemens*, *1998*; *Clemens et al.*, *1999*]). In his thesis, *Pinder* [*1998*] treated the numerical FIT modeling of coupled electromagnetic thermodynamic effects (see also [*Clemens et al.*, *2000*; *van Rienen*, *2001a*]). Based on these developments, commercial software packages are available, for example, the CST *Microwave Studio*™, CST *Design Studio*™, and *MAFIA 4* [*CST*, 2001] (note that *MAFIA* is an acronym for Maxwell's equations solved with the finite integration algorithm). A short discussion of the relationship between the FIT approach and Nédélec or edge elements used in the FE method [*Volakis et al.*, *1998*] can be found in *van Rienen* [*2001a*, *b*]. *Bossavit* [*1998*, *2001*] presented a more comprehensive discussion on edge elements and the generalized Whitney elements (Whitney forms). Analogous to FIT, the mixed FE method and the FE method with Whitney forms use a

dual-cell complex as well, which insures a consistent formulation. A tight link between FIT and mixed FEM, in the sense of differential geometry, is still an open problem for research [*van Rienen*, *2001b*].

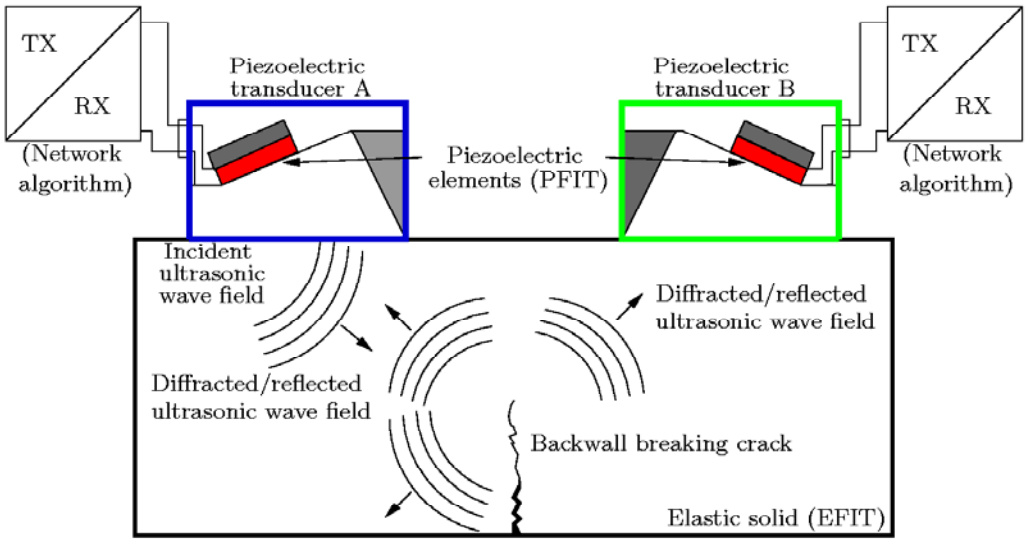


**Figure 2.** A typical setup applied in nondestructive testing/material characterization with ultrasonic wave fields: a steel block with a perfect scatterer (back-wall-breaking crack with stress-free boundary). TX: transmitter; RX: receiver.

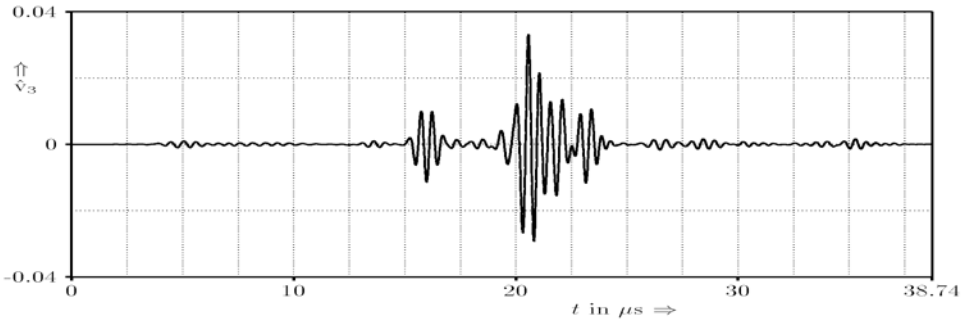


**Figure 3.** A typical time history of a transient echo signal (A-scan; A: amplitude), received in a monostatic experiment: the echo signal from the ultrasonic scattering of a 45° shear wave by a back-wall-breaking crack (see Figure 2), computed with the EFIT.

In time-domain electromagnetics, the resulting discrete grid equations of FIT are, at least in "some" cases, identical to the discrete equations derived with the classical Yee method. This was introduced in the mid-1960s [*Yee*, *1966*], and uses a coordinate-based staggered grid system and the famous Yee cell. In general, FIT includes the Yee method as a subset. In contrast to FIT, which is applied to the integral form of the field equations, the original Yee method is applied to the differential form of the governing equations: in electromagnetism, to the Maxwell curl

equations. Today, Yee's method is well known as the Finite-Difference Time-Domain (FDTD) Method [*Morgan*, *1989*; *Kunz and Luebbers*, *1993*; *Taflove*, *1998*; *Taflove and Hagness*, *2000*; *Sullivan*, *2000*; *fdtd.org*, *2001*]. *Yee et al.* [*1992*] also started from the integral form of Maxwell's equations, and derived a conformal FDTD method (see also [*Yee and Chen*, *1997a,b*). The ideas of the FDTD method can also be applied to other wave-field phenomena. For example, *Sullivan* [*2000*] described the application of the FDTD in (linear) acoustics and quantum mechanics. Independent of these developments in electromagnetism, *Virieux* [*1984*, *1986*] developed a similar method in elastodynamics, which uses all six components of the Cauchy stress tensor and all three components of the particle velocity vector. *Schröder and Scott* [*2000*] and *Scott et al.* [*2001*] utilized this technique to study the interaction of electromagnetic and elastodynamic waves for the application of buried land-mine detection. Historically, in the mid-1970s, *Madariaga* [*1976*] introduced the FDTD method on a staggered grid in elastodynamics. *Saenger et al*. [*2000*] proposed a modified version of this approach. As in the electrodynamics case, the elastodynamic FDTD scheme is contained in EFIT as a subset.

*Fellinger and Langenberg* [*1990*] adapted Weiland's ideas to the governing equations of ultrasonic waves in solids, and developed a numerical procedure called the Elastodynamic Finite Integration Technique (EFIT) (see also [*Fellinger*, *1991*; *Fellinger and Marklein*, *1991*; *Fellinger et al.*, *1995*]). The acoustic pendant to EFIT, AFIT, is generally derived by applying FIT to the governing equations of acoustic waves in integral form [*Marklein and Fellinger*, *1991*; *Marklein*, *1997*]. Stimulated by these developments, *Wolter* [*1995*] and *Bihn* [*1998*] implemented preliminary versions of AFIT and EFIT in the above-mentioned *MAFIA* code. *Peiffer et al.* [*1997*] and *Schubert et al.* [*1998*] derived a CAFIT and CEFIT algorithm for ultrasonic NDT problems with cylindrical symmetry (see also [*Schubert*, *2000*; *Schubert et al.*, *2001*]). AFIT and EFIT have been further developed throughout the last decade to handle more complex media and geometries [*Fellinger et al*., *1995*; *Marklein et al*., *1995*, *1996*, *1997*, *1998*; *Marklein*, *1997*, *2000a*, *b*; *Marklein and Langenberg*, *1998*]. Today, AFIT and EFIT are widely used as well-accepted quantitative modeling tools in nondestructive testing [*Langenberg et al*., *1993*, *1997*, *1999*, *2000*, *2002*]. *Schubert and Köhler* [*2001*] extended EFIT to the nonlinear case. The electromagnetic counterpart of AFIT and EFIT is called EMFIT, and has been applied to diffraction problems [*Langenberg and Marklein*, *1994*] and homogeneous anisotropic uniaxial and biaxial cases [*Marklein et al.*, *1996*; *Marklein*, *1997*]. The acoustic, electromagnetic, elastodynamic, and piezoelectric cases are treated in a unified formulation in *Marklein* [*1997*] and *Marklein et al.*, [*1997*, *2000a*], as well as extended by the coupled electromagnetic-ultrasonic case in *Marklein* [*2000b*].

Recent contributions to numerical modeling in electromagnetics can be found in the book edited by *Teixeira* [*2001*], which includes, among others, the following contributions: *Bossavit* [*2001*], *Clemens and Weiland* [*2001*], *Mattiussi* [*2001*], *Tonti* [*2001b*], *Schuhmann and Weiland* [*2001*], and *van Rienen* [*2001b*]. *Mattiussi* [*1997*, *2000*] gives an overview of various methods applied to solve physical field problems using concepts of algebraic topology. From the viewpoint of topology, *Teixeira and Chew* [*1999a*] present a lattice theory for electromagnetism (see also [*Teixeira and Chew*, *1999b*]).

In the following, we present the application of the "original" FIT, using the local wave field components (see, e.g., [*Weiland*, *1977*; *Fellinger*, *1991*; *Marklein*, *1997*, *2000a*, *b*]), like the discrete field components of the electric field strength and magnetic flux density, instead of global physical quantities, like the electric voltage and the magnetic flux (see, e.g., [*Weiland*, *1996*]). (Note that the derivation presented can be easily reformulated in terms of global physical quantities.) We start with the three uncoupled cases – the acoustic, electromagnetic, and

elastodynamic cases – and then turn to the coupled piezoelectric and electromagnetic-ultrasonic cases, where we make use of the electro-quasistatic (EQS) approximation in the piezoelectric case, and the magneto-quasistatic (MQS) approximation in the electromagnetic-ultrasonic case [*Haus and Melcher*, *1989*]. Both approximations can be considered to be low-frequency approximations of Maxwell's equations in the electromagnetic part of the derived piezoelectric FIT (PFIT) and the electromagnetic-ultrasonic FIT (EMUSFIT) algorithm [*Marklein*, *1997*, *2000a*, *b*; *Langenberg et al.*, *2002*]. Typical examples for coupled field problems are the piezoelectric and electromagnetic-ultrasonic transducers, as shown in Figure 18 (in Section 4). These are applied, e.g., in nondestructive testing (NDT) for the excitation and reception of ultrasonic waves. These ultrasonic antennas rely on the (linear) piezoelectric effect, the (linear) piezo-magnetic effect, the Lorentz force generation, and Ohm's law for moving media.

## 3. ACOUSTIC, ELECTROMAGNETIC, ELASTODYNAMIC, AND COUPLED WAVE FIELDS

### 3.1 FUNDAMENTALS OF ACOUSTIC, ELECTROMAGNETIC, ELASTODYNAMIC WAVE FIELDS

This section summarizes the governing equations, constitutive equations, transition/ continuity and boundary conditions in a unified way. Let $\underline{\mathbf{R}} = x_1 \underline{\mathbf{e}}_1 + x_2 \underline{\mathbf{e}}_2 + x_3 \underline{\mathbf{e}}_3 = x_i \underline{\mathbf{e}}_i$ be the position vector in Cartesian coordinates $x_i$, $i = 1,2,3$, with the three orthonormal unit vectors $\underline{\mathbf{e}}_i$, $i = 1,2,3$, in the three-dimensional Euclidean space $\mathbb{R}^3$, and $t$ being the time. Euclidean vectors, dyads, triads, and tetrads – in general, tensors of $n$th rank – are written as boldface letters underlined with one, two, three, and four lines. Boldface letters in curly and squared brackets denote algebraic vectors and matrices.

The governing field equations of (linear) acoustics, electromagnetics, and (linear) elastodynamics read, in differential form [*Miklowitz*, *1980*; *Ben-Menahem and Singh*, *1981*; *Chen*, *1983*; *Achenbach*, *1984*; *Auld*, *1990*; *de Hoop*, *1995*; *Marklein*, *1997*, *2000a*, *b*; *Royer and Dieulesaint*, *2000a*]:

(Acoustics)
$$\frac{\partial}{\partial t} \underline{\mathbf{j}}(\underline{\mathbf{R}}, t) = -\nabla p(\underline{\mathbf{R}}, t) + \underline{\mathbf{f}}(\underline{\mathbf{R}}, t) \tag{1}$$

$$\frac{\partial}{\partial t} S(\underline{\mathbf{R}}, t) = \nabla \bullet \underline{\mathbf{v}}(\underline{\mathbf{R}}, t) + h(\underline{\mathbf{R}}, t) \tag{2}$$

(Electromagnetics)
$$\frac{\partial}{\partial t} \underline{\mathbf{B}}(\underline{\mathbf{R}}, t) = -\nabla \times \underline{\mathbf{E}}(\underline{\mathbf{R}}, t) - \underline{\mathbf{J}}_{\mathrm{m}}(\underline{\mathbf{R}}, t) \tag{3}$$

$$\frac{\partial}{\partial t} \underline{\mathbf{D}}(\underline{\mathbf{R}}, t) = \nabla \times \underline{\mathbf{H}}(\underline{\mathbf{R}}, t) - \underline{\mathbf{J}}_{\mathrm{e}}(\underline{\mathbf{R}}, t) \tag{4}$$

(Elastodynamics) $$\frac{\partial}{\partial t}\underline{\mathbf{j}}(\underline{\mathbf{R}},t) = \nabla\bullet\underline{\underline{\mathbf{T}}}(\underline{\mathbf{R}},t) + \underline{\mathbf{f}}(\underline{\mathbf{R}},t) \tag{5}$$

$$\frac{\partial}{\partial t}\underline{\underline{\mathbf{S}}}(\underline{\mathbf{R}},t) = \mathrm{sym}\{\nabla\underline{\mathbf{v}}(\underline{\mathbf{R}},t)\} + \underline{\underline{\mathbf{h}}}(\underline{\mathbf{R}},t) \tag{6}$$

| | | | |
|---|---|---|---|
| $p$ [N/m$^2$] | Pressure | $\underline{\mathbf{j}}$ [Ns/m$^3$] | Momentum density vector |
| $\underline{\mathbf{v}}$ [m/s] | Particle velocity vector | $S$ [1] | Scalar deformation |
| $\underline{\mathbf{f}}$ [N/m$^3$] | Volume force density vector | $h$ [1/s] | Injected deformation rate |
| $\underline{\mathbf{E}}$ [V/m] | Electric field strength vector | $\underline{\mathbf{H}}$ [A/m] | Magnetic field strength vector |
| $\underline{\mathbf{D}}$ [As/m$^2$] | Electric flux density vector | $\underline{\mathbf{B}}$ [Vs/m$^2$] | Magnetic flux density vector |
| $\underline{\mathbf{J}}_\mathrm{e}$ [A/m$^2$] | Electric current density vector | $\underline{\mathbf{J}}_\mathrm{m}$ [V/m$^2$] | Magnetic current density vector |
| $\underline{\underline{\mathbf{T}}}$ [N/m] | Cauchy's stress tensor of 2nd rank (dyad) | $\underline{\mathbf{j}}$ [Ns/m$^3$] | Momentum density vector |
| $\underline{\mathbf{v}}$ [m/s] | Particle velocity vector | $\underline{\underline{\mathbf{S}}}$ [1] | Deformation tensor of 2nd rank (dyad) |
| $\underline{\mathbf{f}}$ [N/m$^3$] | Volume force density vector | $\underline{\underline{\mathbf{h}}}$ [1/s] | Injected deformation rate tensor of 2nd rank (dayd) |

The gradient operator is indicated by the symbol "$\nabla$," which is called the del or nabla or Hamilton operator [*Tai*, *1997*]. The divergence and curl operators are denoted by "$\nabla\bullet$" and "$\nabla\times$," respectively. The dot "$\bullet$" accounts for the single scalar product – single contraction of adjacent indices – and the cross "$\times$" mark is the cross product. No dots between vectors/tensors mean a dyadic product. This coordinate-free approach, in electromagnetics [*Chen*, *1983*] and in elastodynamics [*Ben-Menahem and Singh*, *1981*], stands in contrast to the widely used indicial notation, such as used by *de Hoop* [*1995*]. Let $\underline{\underline{\mathbf{D}}}(\underline{\mathbf{R}},t) = \nabla\underline{\mathbf{v}}(\underline{\mathbf{R}},t)$; then, the symmetric part of this dyad is indicated by $\mathrm{sym}\{\underline{\underline{\mathbf{D}}}(\underline{\mathbf{R}},t)\} = \frac{1}{2}\left[\underline{\underline{\mathbf{D}}}(\underline{\mathbf{R}},t) + \underline{\underline{\mathbf{D}}}^{21}(\underline{\mathbf{R}},t)\right]$, which is sometimes denoted by $\nabla_\mathrm{s}$. The upper indicial notation "21" refers to the reordering of the unit vectors, which, for a dyad, is equivalent to the transposition, i.e., $\left[\underline{\mathbf{n}}\,\underline{\mathbf{v}}(\underline{\mathbf{R}},t)\right]^{21} = \underline{\mathbf{v}}(\underline{\mathbf{R}},t)\,\underline{\mathbf{n}}$. The dyads $\underline{\underline{\mathbf{T}}}(\underline{\mathbf{R}},t)$, $\underline{\underline{\mathbf{S}}}(\underline{\mathbf{R}},t)$, and $\underline{\underline{\mathbf{h}}}(\underline{\mathbf{R}},t)$ are symmetric, i.e., $\underline{\underline{\mathbf{T}}}(\underline{\mathbf{R}},t) = \underline{\underline{\mathbf{T}}}^{21}(\underline{\mathbf{R}},t)$.

Equations (1) and (2) are the linear vectorial Newton's law of motion and the scalar law of deformation rate, which are the governing field equations of (linear) acoustic waves in non-viscid fluids and gases. Equations (3) and (4) are the first two vectorial Maxwell's equations, Faraday's induction law and Ampère-Maxwell's circuital law, which are the governing field equations of electromagnetic waves. Equations (5) and (6) are the linear vectorial Cauchy-Newton's law of motion and the tensorial law of deformation rate, which are the governing field equations of (linear) elastodynamic waves in viscid fluids and solids.

Obviously, all three pairs of first-order differential equations – Equations (1) and (2), Equations (3) and (4), and Equations (5) and (6) – exhibit the same structure. We find, on the left-hand side of Equations (1)-(6), a first-order time derivative of one of the field quantities $\underline{\mathbf{j}}(\underline{\mathbf{R}},t)$ and $S(\underline{\mathbf{R}},t)$, $\underline{\mathbf{B}}(\underline{\mathbf{R}},t)$ and $\underline{\mathbf{D}}(\underline{\mathbf{R}},t)$, $\underline{\mathbf{j}}(\underline{\mathbf{R}},t)$ and $\underline{\underline{\mathbf{S}}}(\underline{\mathbf{R}},t)$. On the right-hand side of each equation, we find a differential operator – e.g., the gradient "$\nabla$," divergence "$\nabla\bullet$," curl "$\nabla\times$," and the symmetric gradient operator "$\mathrm{sym}\{\nabla\bullet\}=\nabla_s$" – applied to one of the field quantities $p(\underline{\mathbf{R}},t)$ and $\underline{\mathbf{v}}(\underline{\mathbf{R}},t)$, $\underline{\mathbf{E}}(\underline{\mathbf{R}},t)$ and $\underline{\mathbf{H}}(\underline{\mathbf{R}},t)$, $\underline{\underline{\mathbf{T}}}(\underline{\mathbf{R}},t)$ and $\underline{\mathbf{v}}(\underline{\mathbf{R}},t)$, representing the first-order spatial derivatives as well as source quantities $\underline{\mathbf{f}}(\underline{\mathbf{R}},t)$ and $h(\underline{\mathbf{R}},t)$, (fictitious) $\underline{\mathbf{J}}_{\mathrm{m}}(\underline{\mathbf{R}},t)$ and $\underline{\mathbf{J}}_{\mathrm{e}}(\underline{\mathbf{R}},t)$, $\underline{\mathbf{f}}(\underline{\mathbf{R}},t)$ and $\underline{\underline{\mathbf{h}}}(\underline{\mathbf{R}},t)$ at the outer right of each equation. Note that the Maxwell's Equations (3) and (4) show an additional symmetry: in both equations, the curl operator is applied, which makes the formulation of a duality principle possible.

We now introduce constitutive equations, which characterize properties of the underlying materials. We restrict ourselves in the following derivation to linear, inhomogeneous, anisotropic, instantaneously and locally reacting media.

(Acoustics) $\underline{\mathbf{j}}(\underline{\mathbf{R}},t)=\rho_{a0}(\underline{\mathbf{R}})\underline{\mathbf{v}}(\underline{\mathbf{R}},t)$ (7) $S(\underline{\mathbf{R}},t)=-\kappa(\mathbf{R})p(\underline{\mathbf{R}},t)$ (8)

(Electromagnetics) $\underline{\mathbf{D}}(\underline{\mathbf{R}},t)=\underline{\underline{\boldsymbol{\varepsilon}}}(\mathbf{R})\bullet\underline{\mathbf{E}}(\underline{\mathbf{R}},t)$ (9) $\underline{\mathbf{H}}(\underline{\mathbf{R}},t)=\underline{\underline{\boldsymbol{\nu}}}(\mathbf{R})\bullet\underline{\mathbf{B}}(\underline{\mathbf{R}},t)$ (10)

(Elastodynamics) $\underline{\mathbf{j}}(\underline{\mathbf{R}},t)=\rho_{e0}(\underline{\mathbf{R}})\underline{\mathbf{v}}(\underline{\mathbf{R}},t)$ (11) $\underline{\underline{\mathbf{S}}}(\underline{\mathbf{R}},t)=\underline{\underline{\underline{\underline{\mathbf{s}}}}}(\mathbf{R}):\underline{\underline{\mathbf{T}}}(\underline{\mathbf{R}},t)$ (12)

| | | | |
|---|---|---|---|
| $\rho_{a0}$ [kg/m$^3$] | Acoustic mass density at rest | $\kappa$ [m$^2$/N] | Compressibility |
| $\underline{\underline{\boldsymbol{\varepsilon}}}$ [As/Vm] | Permittivity tensor of 2nd rank (dyad) | $\underline{\underline{\boldsymbol{\nu}}}$ [Am/Vs] | Reluctivity tensor of 2nd rank (dyad) |
| $\rho_{e0}$ [kg/m$^3$] | Elastic mass density at rest | $\underline{\underline{\underline{\underline{\mathbf{s}}}}}$ [m$^2$/N] | Compliance tensor of 4th rank (tetrad) |

The colon "**:**" in Equation (12), which is the generalized Hooke law [*Miklowitz*, *1980*], denotes the double-scalar product with the property $\underline{\mathbf{a}}\,\underline{\mathbf{b}}:\underline{\mathbf{c}}\,\underline{\mathbf{d}}=(\underline{\mathbf{b}}\bullet\underline{\mathbf{c}})(\underline{\mathbf{a}}\bullet\underline{\mathbf{d}})$, i.e., a double contraction of two index pairs, with the top dot tied to the adjacent indices, again. Of course, we could also treat more complex media, for instance, dissipative, inhomogeneous, anisotropic solid media. Examples can be found in the references listed at the end of this section. Coordinate-free representations of the material tensors can be found, for example, in *Marklein* [*1997*].

For inhomogeneous materials with interfaces or for boundary-value problems, it is essential that the underlying transition/continuity or boundary conditions are insured. Suppose two media, (1) and (2), with different materials are separated by an interface, *I*, with unit-normal $\underline{\mathbf{n}}$ pointing from medium (1) into medium (2); then, for $\underline{\mathbf{R}}\in I$, we find for the three different cases:

(Acoustics)
$$\underline{\mathbf{n}}p^{(2)}(\underline{\mathbf{R}},t)-\underline{\mathbf{n}}p^{(1)}(\underline{\mathbf{R}},t)=\begin{cases}\underline{\mathbf{t}}(\underline{\mathbf{R}},t) & \text{with interface sources}\\ \underline{\mathbf{0}} & \text{source-free}\end{cases} \tag{13}$$

$$\mathbf{n}\bullet\underline{\mathbf{v}}^{(2)}(\underline{\mathbf{R}},t)-\mathbf{n}\bullet\underline{\mathbf{v}}^{(1)}(\underline{\mathbf{R}},t)=\begin{cases}-g(\underline{\mathbf{R}},t) & \text{with interface sources}\\ 0 & \text{source-free}\end{cases} \tag{14}$$

(Electromagnetics)
$$\underline{\mathbf{n}}\times\underline{\mathbf{E}}^{(2)}(\underline{\mathbf{R}},t)-\underline{\mathbf{n}}\times\underline{\mathbf{E}}^{(1)}(\underline{\mathbf{R}},t)=\begin{cases}-\underline{\mathbf{K}}_{\mathrm{m}}(\underline{\mathbf{R}},t) & \text{with interface sources}\\ \underline{\mathbf{0}} & \text{source-free}\end{cases} \tag{15}$$

$$\underline{\mathbf{n}}\times\underline{\mathbf{H}}^{(2)}(\underline{\mathbf{R}},t)-\underline{\mathbf{n}}\times\underline{\mathbf{H}}^{(1)}(\underline{\mathbf{R}},t)=\begin{cases}\underline{\mathbf{K}}_{\mathrm{e}}(\underline{\mathbf{R}},t) & \text{with interface sources}\\ \underline{\mathbf{0}} & \text{source-free}\end{cases} \tag{16}$$

(Elastodynamics)
$$\underline{\mathbf{n}}\bullet\underline{\underline{\mathbf{T}}}^{(2)}(\underline{\mathbf{R}},t)-\underline{\mathbf{n}}\bullet\underline{\underline{\mathbf{T}}}^{(1)}(\underline{\mathbf{R}},t)=\begin{cases}-\underline{\mathbf{t}}(\underline{\mathbf{R}},t) & \text{with interface sources}\\ \underline{\mathbf{0}} & \text{source-free}\end{cases} \tag{17}$$

$$\mathrm{sym}\{\underline{\mathbf{n}}\,\underline{\mathbf{v}}^{(2)}(\underline{\mathbf{R}},t)\}-\mathrm{sym}\{\underline{\mathbf{n}}\,\underline{\mathbf{v}}^{(1)}(\underline{\mathbf{R}},t)\}=\begin{cases}-\underline{\underline{\mathbf{g}}}(\underline{\mathbf{R}},t) & \text{with interface sources}\\ \underline{\underline{\mathbf{0}}} & \text{source-free}\end{cases} \tag{18}$$

| | | | |
|---|---|---|---|
| $\underline{\mathbf{t}}$ [N/m$^2$] | Surface density of force vector | $g$ [m/s] | Surface density of injected deformation rate |
| $\underline{\mathbf{K}}_{\mathrm{m}}$ [V/m] | Magnetic surface current density vector | $\underline{\mathbf{K}}_{\mathrm{e}}$ A/m] | Surface density of electric current vector |
| $\underline{\mathbf{t}}$ [N/m$^2$] | Surface density of force vector | $\underline{\underline{\mathbf{g}}}$ [m/s] | Source density of injected deformation rate tensor of 2nd rank (dyad) |

In general, the surface sources on the right-hand side of Equations (13)-(18) are field-independent sources. If we replace medium (1) by a medium that is field-free, boundary conditions are needed for the fields, which are directly obtained from Equations (13)-(18) by deleting all field quantities with a superscript (1) and dropping the superscript (2). Then, the interface sources on the right-hand side of Equations (13)-(18) vanish or define field-dependent sources. For instance, on a perfectly electrically conducting (PEC) boundary, $\underline{\mathbf{n}}\times\underline{\mathbf{E}}(\underline{\mathbf{R}},t)=\underline{\mathbf{0}}$ holds, and then $\underline{\mathbf{K}}_{\mathrm{e}}(\underline{\mathbf{R}},t)=\underline{\mathbf{n}}\times\underline{\mathbf{H}}(\underline{\mathbf{R}},t)$ defines a field-dependent induced electric surface current density at the boundary. Note that in the discretization process, which is discussed below, only discrete field components that are continuous according to the continuity/transition conditions of Equations (13)-(18) should be allocated at the interfaces of material cells filled with different material properties, in order to implicitly insure the interface/continuity condition.

For the utilization of the Finite Integration Technique, we write down the governing field equations, Equations (1)-(6), in integral form by making use of Gauss' and Stokes' integral theorem, and insert the constitutive equations, Equations (7)-(12), as well as adding time-integration schemes:

(Acoustics)
$$\iiint_V \rho_{a0}(\underline{\mathbf{R}})\dot{\underline{\mathbf{v}}}(\underline{\mathbf{R}},t)dV = -\oiint_{S=\partial V} p(\underline{\mathbf{R}},t)\underline{\mathbf{dS}} + \iiint_V \underline{\mathbf{f}}(\underline{\mathbf{R}},t)dV \tag{19}$$

$$\underline{\mathbf{v}}(\underline{\mathbf{R}},t) = \underline{\mathbf{v}}(\underline{\mathbf{R}},t_0) + \int_{t_0}^{t} \dot{\underline{\mathbf{v}}}(\underline{\mathbf{R}},t')dt' \tag{20}$$

$$\iiint_V \kappa(\underline{\mathbf{R}})\dot{p}(\underline{\mathbf{R}},t)dV = -\oiint_{S=\partial V} \underline{\mathbf{v}}(\underline{\mathbf{R}},t) \bullet \underline{\mathbf{dS}} - \iiint_V h(\underline{\mathbf{R}},t)dV \tag{21}$$

$$p(\underline{\mathbf{R}},t) = p(\underline{\mathbf{R}},t_0) + \int_{t_0}^{t} \dot{p}(\underline{\mathbf{R}},t')dt' \tag{22}$$

(Electromagnetics)
$$\iint_S \dot{\underline{\mathbf{B}}}(\underline{\mathbf{R}},t) \bullet \underline{\mathbf{dS}} = -\oint_{C=\partial S} \underline{\mathbf{E}}(\underline{\mathbf{R}},t) \bullet \underline{\mathbf{dR}} - \iint_S \underline{\mathbf{J}}_{\mathrm{m}}(\underline{\mathbf{R}},t) \bullet \underline{\mathbf{dS}} \tag{23}$$

$$\underline{\mathbf{B}}(\underline{\mathbf{R}},t) = \underline{\mathbf{B}}(\underline{\mathbf{R}},t_0) + \int_{t_0}^{t} \dot{\underline{\mathbf{B}}}(\underline{\mathbf{R}},t')dt' \tag{24}$$

$$\iint_S [\underline{\underline{\boldsymbol{\varepsilon}}}(\underline{\mathbf{R}}) \bullet \dot{\underline{\mathbf{E}}}(\underline{\mathbf{R}},t)] \bullet \underline{\mathbf{dS}} = \oint_{C=\partial S} [\underline{\underline{\boldsymbol{\nu}}}(\underline{\mathbf{R}}) \bullet \underline{\mathbf{B}}(\underline{\mathbf{R}},t)] \bullet \underline{\mathbf{dR}} - \iint_S \underline{\mathbf{J}}_{\mathrm{e}}(\underline{\mathbf{R}},t) \bullet \underline{\mathbf{dS}} \tag{25}$$

$$\underline{\mathbf{E}}(\underline{\mathbf{R}},t) = \underline{\mathbf{E}}(\underline{\mathbf{R}},t_0) + \int_{t_0}^{t} \dot{\underline{\mathbf{E}}}(\underline{\mathbf{R}},t')dt' \tag{26}$$

(Elastodynamics)
$$\iiint_V \rho_{e0}(\underline{\mathbf{R}})\dot{\underline{\mathbf{v}}}(\underline{\mathbf{R}},t)dV = \oiint_{S=\partial V} \underline{\underline{\mathbf{T}}}(\underline{\mathbf{R}},t) \bullet \underline{\mathbf{dS}} + \iiint_V \underline{\mathbf{f}}(\underline{\mathbf{R}},t)dV \tag{27}$$

$$\underline{\mathbf{v}}(\underline{\mathbf{R}},t) = \underline{\mathbf{v}}(\underline{\mathbf{R}},t_0) + \int_{t_0}^{t} \dot{\underline{\mathbf{v}}}(\underline{\mathbf{R}},t')dt' \tag{28}$$

$$\iiint_V \underline{\underline{\underline{\mathbf{s}}}}(\underline{\mathbf{R}}) : \dot{\underline{\underline{\mathbf{T}}}}(\underline{\mathbf{R}},t)dV = \oiint_{S=\partial V} \mathrm{sym}\{\underline{\mathbf{n}}\underline{\mathbf{v}}(\underline{\mathbf{R}},t)\}dS + \iiint_V \underline{\underline{\mathbf{h}}}(\underline{\mathbf{R}},t)dV \tag{29}$$

$$\underline{\underline{\mathbf{T}}}(\underline{\mathbf{R}},t) = \underline{\underline{\mathbf{T}}}(\underline{\mathbf{R}},t_0) + \int_{t_0}^{t} \dot{\underline{\underline{\mathbf{T}}}}(\underline{\mathbf{R}},t')dt' \,, \tag{30}$$

where $S = \partial V$ is the closed surface of the volume $V$. These three sets of Equations (19)-(22), (23)-(26), and (27)-(30) already illustrate the characteristic leapfrog structure.

### 3.2 Derivations and Essentials of the Numerical Codes: AFIT, EMFIT, and EFIT

A typical transient simulation task is described by a known/assumed geometry and material configuration, as well as boundary conditions and antenna characteristics for the emitting and receiving modes. Different types of grid complexes can be used for the discretization in space, as

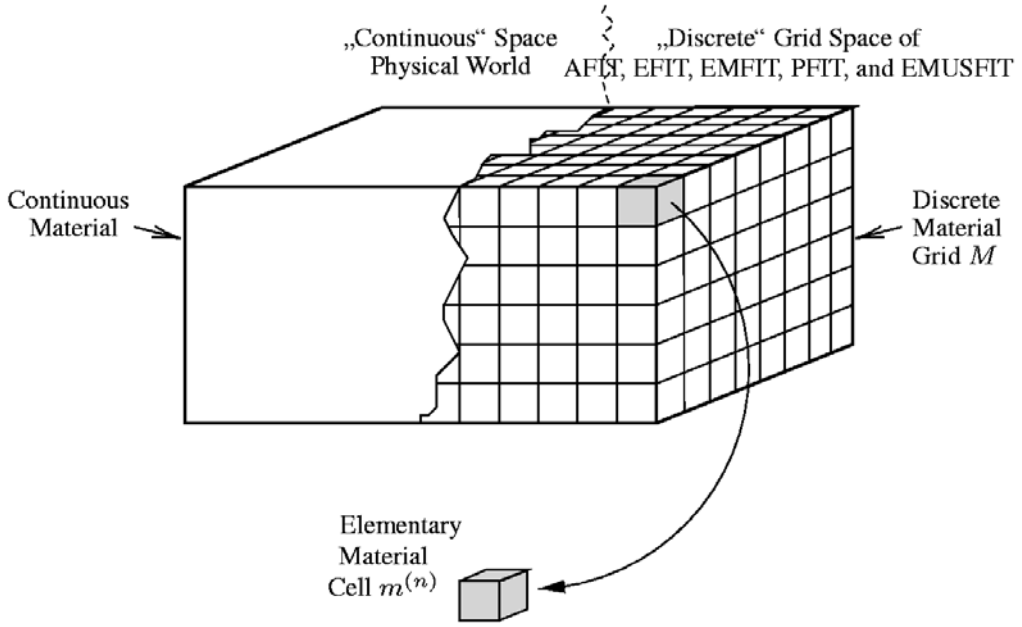


**Figure 4.** A discretization of the material in elementary material cells $m^{(n)}$, defining the material grid *M*.

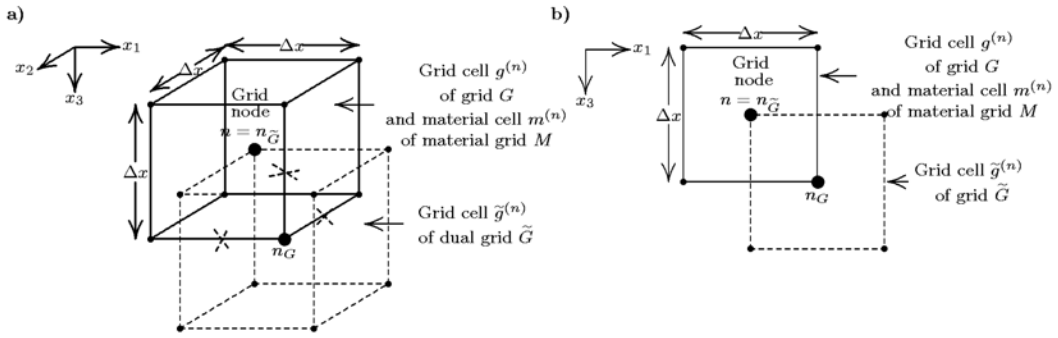


**Figure 5.** The grid complex with the grid, $G$ (primary grid), and its dual grid, $\tilde{G}$ (secondary grid), as well as the material grid: (a) three-dimensional case and (b) two-dimensional case.

indicated in Figure 4, e.g., a dual-coordinate-based cell complex, consisting of cubic cells, or dual simplicial cell complexes consisting of Delaunay triangles and Voronoi polygons (e.g., [*Marklein*, *1997*; *Tonti*, *2001a*, *b*]). The reader is also referred to *Schuhmann* [1999], *Hilgner* [2001], and *van Rienen* [*2001a*, *b*]. In the following we restrict ourselves to a regular cubic cell complex consisting of a material grid complex $M$, a primal grid complex $G$, and a dual grid complex $\widetilde{G}$ as shown in Figure 5. The original idea of *Weiland* [*1977*] was to use the multidimensional midpoint rule to

approximate the integral appearing in the governing equations. For a one-dimensional integral, as shown in Figure 6, we find the following approximation by standard Taylor-series expansion:

$$\int_{x_0}^{x_0+\Delta x} f(x)dx = f\left(x_0+\frac{\Delta x}{2}\right)\Delta x + O\left[(\Delta x)^3\right] \approx f\left(x_0+\frac{\Delta x}{2}\right)\Delta x\,, \tag{31}$$

where $O\left[(\Delta x)^3\right]$ denotes the approximation error. Note that the same approximation is used to discretize the one-dimensional time integral, see, e.g., Equation (20). Approximations of two- and three-dimensional integrals, like surface and volume integrals, are derived in a similar way (see, e.g., [ *Marklein*, *1997*; *van Rienen*, *2001a*]), which yields

$$\begin{aligned}\int_{y_0}^{y_0+\Delta x}\int_{x_0}^{x_0+\Delta x} f(x,y)\,dx\,dy &= f\left(x_0+\frac{\Delta x}{2},y_0+\frac{\Delta x}{2}\right)(\Delta x)^2 + O\left[(\Delta x)^4\right] \\ &\approx f\left(x_0+\frac{\Delta x}{2},y_0+\frac{\Delta x}{2}\right)(\Delta x)^2 \end{aligned} \tag{32}$$

$$\begin{aligned}\int_{z_0}^{z_0+\Delta x}\int_{y_0}^{y_0+\Delta x}\int_{x_0}^{x_0+\Delta x} f(x,y,z)\,dx\,dy\,dz &= f\left(x_0+\frac{\Delta x}{2},y_0+\frac{\Delta x}{2},z_0+\frac{\Delta x}{2}\right)(\Delta x)^3 + O\left[(\Delta x)^5\right] \\ &\approx f\left(x_0+\frac{\Delta x}{2},y_0+\frac{\Delta x}{2},z_0+\frac{\Delta x}{2}\right)(\Delta x)^3\,. \end{aligned} \tag{33}$$

A combination of Equations (31) and (32) or Equations (32) and (33), according to the governing Equations (19)-(30), always gives a second-order approximation ( $O\left[(\Delta x)^2\right]$ ).

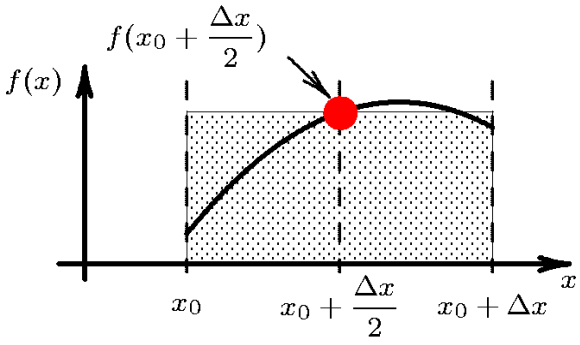


**Figure 6.** The midpoint rule applied to a one-dimensional integral.

The application of the Finite Integration Technique (FIT), using a dual-cell complex in space and time, as shown in Figure 7, yields the following three sets of matrix equations.

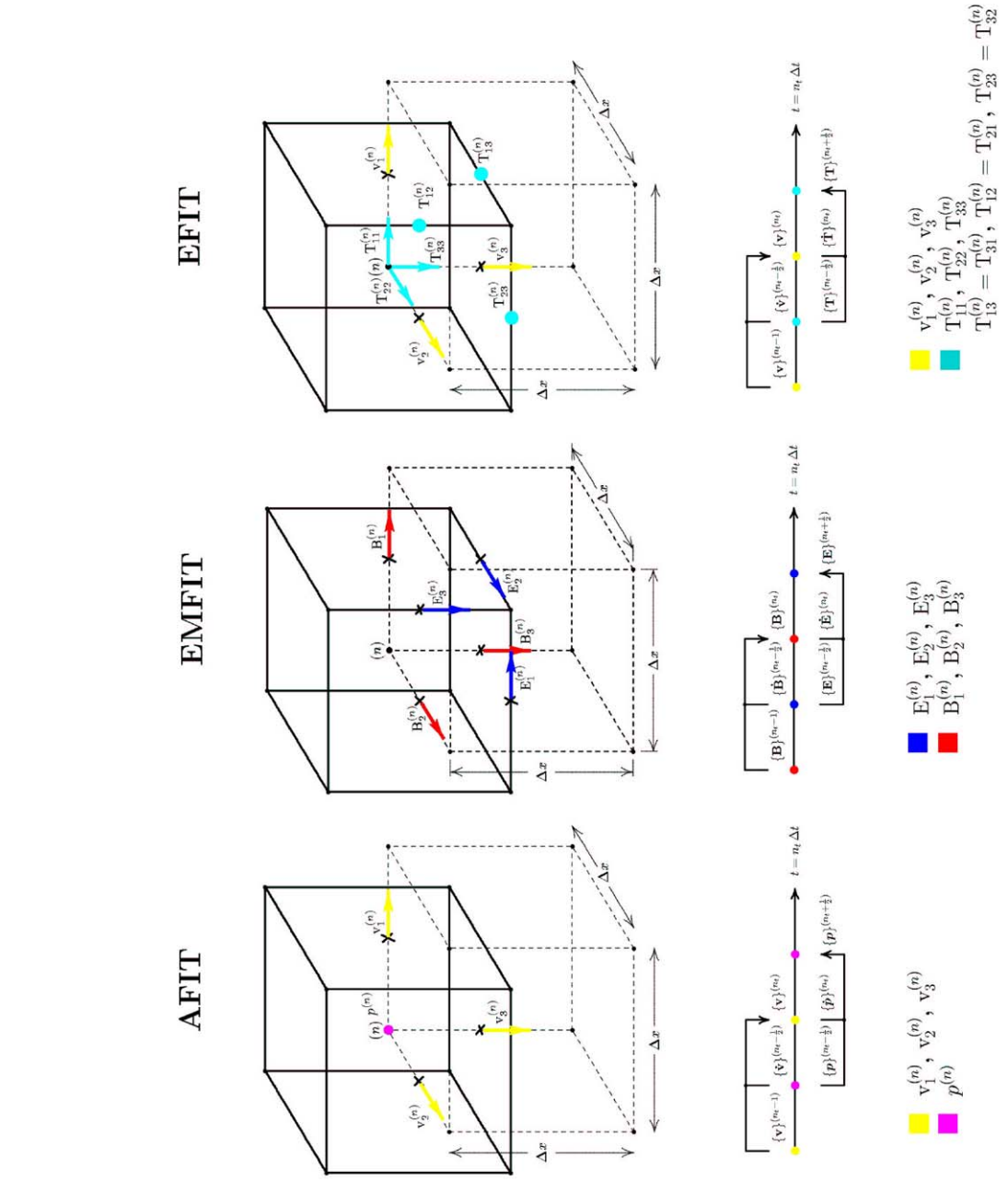


**Figure 7.** The spatial and temporal grid complex of AFIT, EMFIT, and EFIT, and the allocation of the local discrete field quantities (also see Plate 3).

(Acoustics)
$$\{\dot{\mathbf{v}}\}^{(n_t-1/2)} = [\tilde{\boldsymbol{\rho}}_{a0}]^{-1}[\widetilde{\mathbf{R}}]^{-1}[\widetilde{\mathbf{grad}}]\{\mathbf{p}\}^{(n_t-1/2)} + [\tilde{\boldsymbol{\rho}}_{a0}]^{-1}\{\mathbf{f}\}^{(n_t-1/2)} \tag{34}$$

$$\{\mathbf{v}\}^{(n_t)} = \{\mathbf{v}\}^{(n_t-1)} + \Delta t\{\dot{\mathbf{v}}\}^{(n_t-1/2)} \tag{35}$$

$$\{\dot{\wp}\}^{(n_t)} = -[\boldsymbol{\kappa}]^{-1}[\mathbf{div}][\mathbf{R}]^{-1}\{\mathbf{v}\}^{(n_t)} - [\boldsymbol{\kappa}]^{-1}\{\mathbf{h}\}^{(n_t)} \tag{36}$$

$$\{\mathbf{p}\}^{(n_t+1/2)} = \{\mathbf{p}\}^{(n_t-1/2)} + \Delta t\{\dot{\mathbf{p}}\}^{(n_t)} \tag{37}$$

(Electromagnetics)
$$\{\dot{\mathbf{B}}\}^{(n_t-1/2)} = -[\mathbf{R}]^{-1}[\mathbf{curl}]\{\mathbf{E}\}^{(n_t-1/2)} - \{\mathbf{J}_m\}^{(n_t-1/2)} \tag{38}$$

$$\{\mathbf{B}\}^{(n_t)} = \{\mathbf{B}\}^{(n_t-1)} + \Delta t\{\dot{\mathbf{B}}\}^{(n_t-1/2)} \tag{39}$$

$$\{\dot{\mathbf{E}}\}^{(n_t)} = [\tilde{\boldsymbol{\varepsilon}}]^{-1}[\widetilde{\mathbf{R}}]^{-1}[\widetilde{\mathbf{curl}}][\tilde{\mathbf{v}}]\{\mathbf{B}\}^{(n_t)} - [\tilde{\boldsymbol{\varepsilon}}]^{-1}\{\mathbf{J}_e\}^{(n_t)} \tag{40}$$

$$\{\mathbf{E}\}^{(n_t+1/2)} = \{\mathbf{E}\}^{(n_t-1/2)} + \Delta t\{\dot{\mathbf{E}}\}^{(n_t)} \tag{41}$$

(Elastodynamics)
$$\{\dot{\mathbf{v}}\}^{(n_t-1/2)} = [\tilde{\boldsymbol{\rho}}_{e0}]^{-1}[\widetilde{\mathbf{DIV}}][\widetilde{\mathbf{R}}_{\dot{v}}^{T}][\mathbf{A}_{\dot{v}}^{T}]\{\mathbf{T}\}^{(n_t-1/2)} + [\tilde{\boldsymbol{\rho}}_{e0}]^{-1}\{\mathbf{f}\}^{(n_t-1/2)} \tag{42}$$

$$\{\mathbf{v}\}^{(n_t)} = \{\mathbf{v}\}^{(n_t-1)} + \Delta t\{\dot{\mathbf{v}}\}^{(n_t-1/2)} \tag{43}$$

$$\{\dot{\mathbf{T}}\}^{(n_t)} = [\mathbf{c}][\mathbf{R}_{\dot{T}}^{v}]^{-1}[\mathbf{GRAD}][\mathbf{A}_{\dot{T}}^{v}]\{\mathbf{v}\}^{(n_t)} + \{\mathbf{g}\}^{(n_t)} \tag{44}$$

$$\{\mathbf{T}\}^{(n_t+1/2)} = \{\mathbf{T}\}^{(n_t-1/2)} + \Delta t\{\dot{\mathbf{T}}\}^{(n_t)}. \tag{45}$$

These are the so-called grid equations of AFIT, EMFIT, and EFIT in matrix form, which represent a one-to-one translation to the governing equations. The integer counter, $n_t$, denotes the time step, where the time is given by $t = \Delta t\, n_t$. Each of the above three sets of matrix equations, Equations (34)-(37), (38)-(41), and (42)-(45), represent a marching-on-in-time algorithm of "leap frog" type, which are of second order in space and time ($O\left[(\Delta x)^2\right], O\left[(\Delta t)^2\right]$). In the above matrix equations, $\{\mathbf{v}\}$, $\{\mathbf{p}\}$, $\{\mathbf{f}\}$, $\{\mathbf{h}\}$, $\{\mathbf{B}\}$, $\{\mathbf{E}\}$, $\{\mathbf{J}_m\}$, $\{\mathbf{J}_e\}$, $\{\mathbf{v}\}$, $\{\mathbf{T}\}$, $\{\mathbf{f}\}$, and $\{\mathbf{g}\}$ are algebraic field vectors; $[\tilde{\boldsymbol{\rho}}_{a0}]$, $[\boldsymbol{\kappa}]$, $[\tilde{\boldsymbol{\varepsilon}}]$, $[\tilde{\mathbf{v}}]$, $[\tilde{\boldsymbol{\rho}}_{e0}]$, and $[\mathbf{c}]$ are material matrices; $[\mathbf{R}]$, $[\widetilde{\mathbf{R}}]$, $[\widetilde{\mathbf{R}}_{\dot{v}}^{T}]$, and $[\mathbf{R}_{\dot{T}}^{v}]$ are matrices containing the distances; $[\mathbf{A}_{\dot{v}}^{T}]$ and $[\mathbf{A}_{\dot{T}}^{v}]$ are averaging matrices; and $[\widetilde{\mathbf{grad}}]$, $[\mathbf{div}]$, $[\mathbf{curl}]$, $[\widetilde{\mathbf{curl}}]$, $[\widetilde{\mathbf{DIV}}]$, and $[\mathbf{GRAD}]$ are topological matrix operators containing only the integers $\{-1,0,1\}$, all on the primal and dual grid complex $G$ and $\widetilde{G}$. The topological operators insure essential vector analytic properties in the discrete grid space:

$$\nabla\times\nabla = \underline{\mathbf{0}} \quad \Leftrightarrow \qquad [\mathbf{curl}][\mathbf{grad}] = [\widetilde{\mathbf{curl}}][\widetilde{\mathbf{grad}}] = [\mathbf{0}] \tag{46}$$

$$\nabla \bullet \nabla \times = 0 \;\Leftrightarrow \qquad [\mathbf{div}][\mathbf{curl}] = [\widetilde{\mathbf{div}}][\widetilde{\mathbf{curl}}] = [\mathbf{0}], \tag{47}$$

where the algebraic null matrix is denoted by $[\mathbf{0}]$.

Note that the topological matrix operators $[\mathbf{curl}]$, $[\widetilde{\mathbf{curl}}]$, $[\mathbf{div}]$, and $[\mathbf{grad}]$ in Weiland's notation correspond to $\mathbf{C}$, $\widetilde{\mathbf{C}}$, $\mathbf{S}$, and $-\tilde{\mathbf{S}}^{\mathrm{T}}$ [*Weiland*, *1996*]. In practice, the computation of Equations (34) and (35), for instance, in two steps is avoided by inserting Equation (34) into Equation (35). This is also valid for Equations (36) and (37), and so on.

The transition/continuity conditions are implicitly ensured, and perfect and absorbing boundary conditions can easily be implemented in the discrete grid equations. As an example for an absorbing boundary condition, the perfectly matched layer (PML) can be implemented straightforwardly. *Berenger* [*1994*] introduced the PML in electrodynamics in the mid-1990s. *Chew and Liu* [*1996*] extended the PML to the elastodynamic case, and *Yuan et al.* [*1999*] proposed the PML in acoustics. *Teixeira and Chew* [*1999b*] presented a modern treatment of the PML in electromagnetics using differential forms.

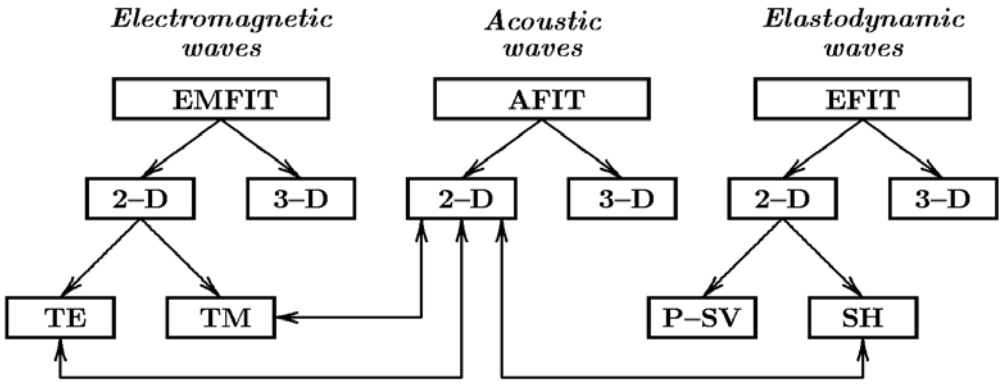


**Figure 8.** The numerical tools EMFIT, AFIT, and EFIT, and their interrelationships in the two-dimensional case.

AFIT, EMFIT, and EFIT are explicit hyperbolic time-domain solvers of the marching-on-in-time type. Figure 8 shows the interrelationships of the three- and two-dimensional codes. For instance, in two-dimensional electromagnetics, we distinguish between the transverse electric (TE) and the transverse magnetic (TM) cases, and in two-dimensional elastodynamics, we distinguish between the pressure-shear vertical (P-SV) and shear horizontal (SH) cases. All scalar cases – the TE, TM, and SH cases – are strongly related to the two-dimensional acoustic case (see also the numerical examples in Sections 3.3.1 and 3.3.2).

One can also consider the above discretization procedure in the language of differential forms and algebraic topology. Then, the spatial discretization process is split into two steps. In the first step, global field quantities – like electric and magnetic voltages, as well as fluxes, particle fluxes, and forces assigned to geometric objects, e.g., lines $L$ and $\widetilde{L}$, surfaces $S$ and $\widetilde{S}$, and volumes

$V$ and $\widetilde{V}$ – are introduced. This will generate an exact set of discrete metric-free matrix equations as an exact one-to-one translation of the analytical field equations. In the second step, approximations are needed for the discretization of the constitutive equations. The resulting operators can be identified as discrete Hodge operators in the language of differential forms, which contain the metric of the dual cell complex (see, for example, [*Clemens and Weiland*, *2001*]). It is also possible to work with quantities assigned to space-time objects, as presented in a different approach by *Mattiussi* [*1997*, *2000*, *2001*] and *Tonti* [*2001a*, *b*] (see also [*Teixeira*, *2001*; *Discrete Physics*, *2001*]).

Stability of the above schemes is insured for a regular Cartesian-grid complex if the following $n$-dimensional – with the dimension $n \in \{1,2,3\}$ – Courant-Friedrichs-Lewy (CFL) condition [*Courant et al.*, *1928*; *Richtmyer and Morton*, *1967*; *Strikwerda*, *1989*; *Gustafsson et al.*, *1995*] is insured:

$$\Delta t \le \Delta t_{\max} = \frac{1}{\sqrt{n}} \frac{\Delta x}{c_{\max}} \qquad \text{with} \qquad \Delta x \approx \frac{\min \lambda_{\{\mathrm{A,EM,E}\}}}{10}. \tag{48}$$

The time step, $\Delta t$, is a function of the grid cell size, $\Delta x$. The spatial resolution, $\Delta x$, of the regular Cartesian cubic cell complex is a function of the minimum wavelength $\min \lambda_{\{\mathrm{A,EM,E}\}}$ in the acoustic (A), electromagnetic (EM), and elastodynamic (E) case. The time step, $\Delta t$, also depends directly on the maximum propagation velocity, $c_{max}$, which is, in fact, the maximum energy or group velocity in the region of interest. This property is very important if anisotropic materials are under concern [*Fellinger et al*., *1995*; *Marklein et al*., *1995*, *1996*; *Marklein*, *1997*; *Langenberg et al.*, *2002*].

The spatial and temporal discretization introduces numerical errors – like artificial anisotropy, dispersion, and dissipation – even for isotropic, dispersion-free, and non-dissipative materials. For example, for a plane wave propagating in the $\underline{\mathbf{k}} = k_i \underline{\mathbf{e}}_i$ direction, the following dispersion relation holds for the above numerical schemes:

$$\frac{1}{(c\Delta t)^2} \sin^2\left(\frac{\omega \Delta t}{2}\right) = \sum_{i=1}^{n} \frac{1}{(\Delta x)^2} \sin^2\left(\frac{k_i \Delta x}{2}\right), \tag{49}$$

with $c$ being the propagation velocity [*Fang*, *1989*; *Marklein*, *1997*]. In practice, artificial dispersion is one of the main problems, especially if ten thousand time-steps are computed. To compensate for this numerical dispersion, one can use a flux-corrected approach, as proposed by *Fei and Larner* [*1995*].

Further details, numerical results, and applications of AFIT, EMFIT, and EFIT can be found in *Marklein* [*1997*] (see also [*Fellinger and Langenberg*, *1990*; *Marklein and Fellinger*, *1991*; *Fellinger*, *1991*; *Fellinger and Marklein*, *1991*; *Langenberg et al*., *1993*, *1997*, *1999*, *2000*, *2002*; *Langenberg and Marklein*, *1994*; *Fellinger et al*., *1995*; *Marklein et al*., *1995*, *1996*, *1997*, *1998*; *Marklein*, *1997*, *2000a*, *b*; *Schuhmacher*, *1997*; *Marklein and Langenberg*, *1998*; *Kostka*, *1999*; *Halkjær*, *2000*, *Halkjær et al.*, *2000*; *Hannemann*, *2001*]).

### 3.3. NUMERICAL EXAMPLES OF AFIT, EMFIT, AND EFIT

#### 3.3.1 Sommerfeld's Half-Plane Problem Computed with AFIT and EMFIT

Figure 9 displays time-domain snapshots of a time-harmonic TE-polarized plane wave impinging on an infinitely thin perfectly electrically conducting half-plane. This is a classical diffraction problem, called Sommerfeld's half-plane problem [*Born and Wolf*, *1989*], which, in acoustics, is equivalent to a Neumann boundary-value problem for a vanishing normal derivative of the pressure on the half-plane. Modeling results for a time-harmonic plane-wave excitation, computed with 2D-AFIT/2D-TE-EMFIT, are given in the left, middle, and right of Figure 9, respectively. A validation of the numerical results is shown in Figure 10. Snapshots of the transient case for a broadband raised-cosine impulse are displayed in Figure 11. The validation of the FIT results against analytical results is presented in Figure 12.

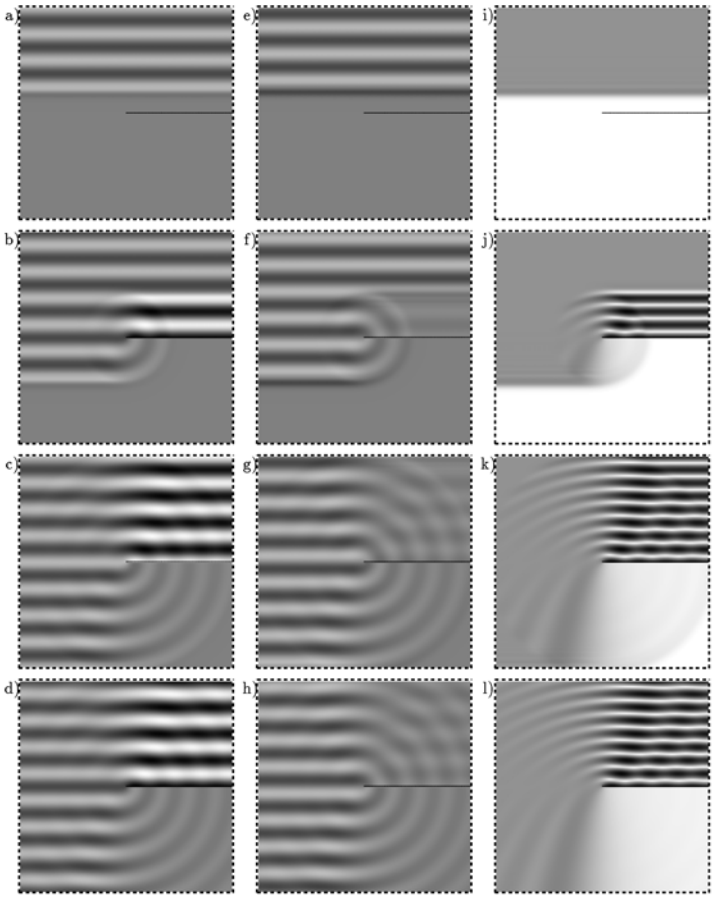


**Figure 9.** Sommerfeld's half-plane diffraction problem: 2D-TE-EMFIT/2D-AFIT simulation results for cosine excitation (left: a, b, c, and d), sine excitation (middle: e, f, g, and h), and the magnitude of both simulations, representing the magnitude of a complex monochromatic excitation (right: i, j, k, and l).

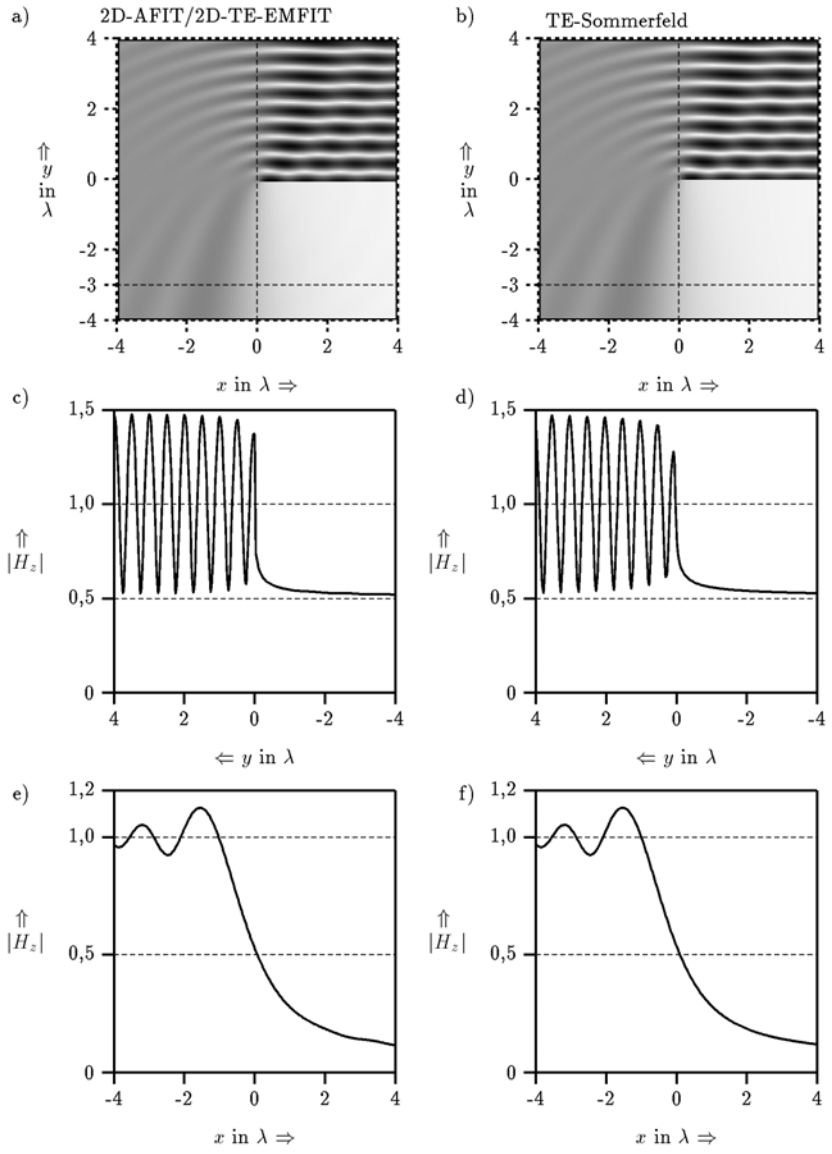


**Figure 10.** Sommerfeld's half-plane diffraction problem: validation of the 2D-TE-EMFIT/2D-AFIT results (left: a, c, and e) against analytical TE-Sommerfeld results (right: b, d, f) for a complex monochromatic excitation. a) Displays the time-domain result after reaching the stationary case compared to the frequency-domain Sommerfeld result; c) and e) as well as d) and f) display vertical and horizontal cross sections.

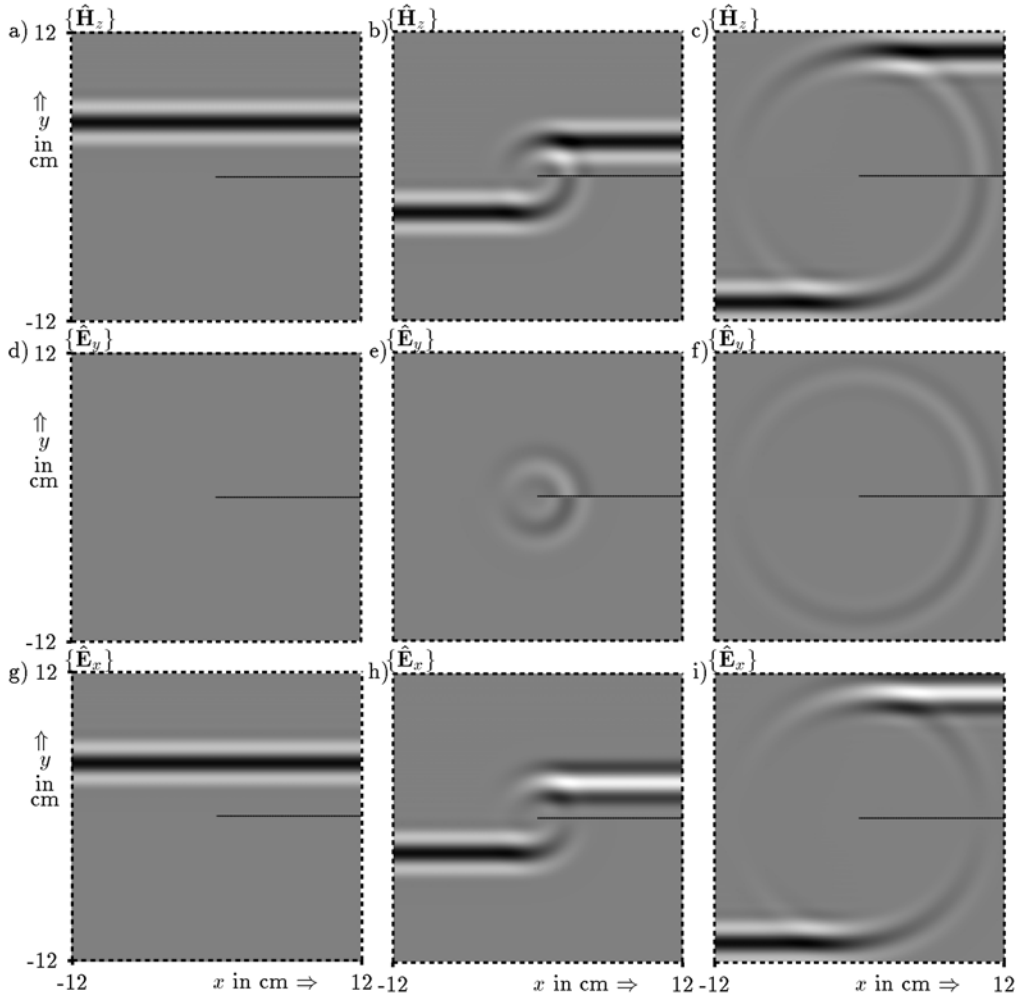


**Figure 11.** 2D-TE-EMFIT/2D-AFIT time-domain field snapshots of the Sommerfeld half-plane diffraction problem in the $xy$ plane: magnetic field strength component $H_z$ (top: a, b, and c), vertical electric field strength component $E_y$ (middle: d, e, and f), and horizontal electric field component $E_x$ (bottom: g, h, and i).

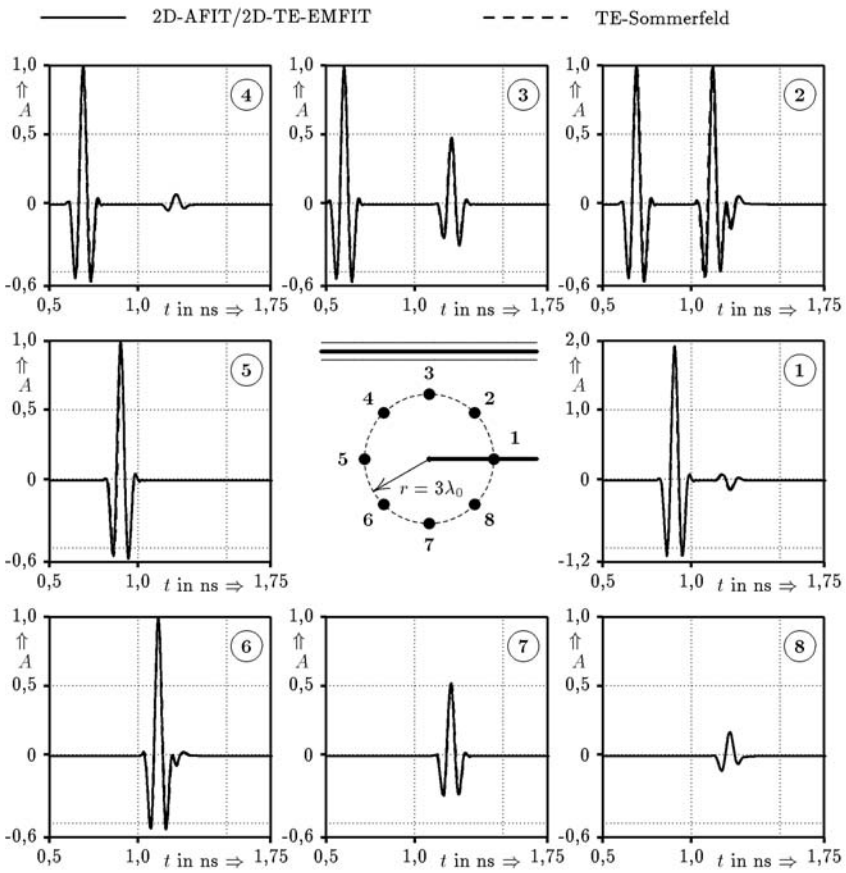


**Figure 12.** Validation of the 2D-TE-EMFIT/2D-AFIT results against TE-Sommerfeld solution: displayed are transient responses received at eight different locations on a circle with radius $r = 3\lambda_0$ centered at the tip of the half-plane, with $\lambda_0$ being the wavelength in free space.

### 3.3.2 Shirai's and Felsen's Open-Ended Waveguide Problem Computed with AFIT and EMFIT

Figures 13 and 14 illustrate the problem attacked by *Shirai and Felsen* [*1987*]: a TE-polarized time-harmonic plane wave impinges and couples into an open-ended waveguide, composed of two infinitely thin perfectly electrically conducting planes. Displayed are time-domain snapshots computed with 2D-TE-EMFIT/2D-AFIT. Their method of solution, which involves an intricate evaluation and decomposition of spectral integrals into rays and modes, is approximately valid for high frequencies. Figure 15 validates the EMFIT/AFIT solution against results obtained with the Shirai and Felsen approach.

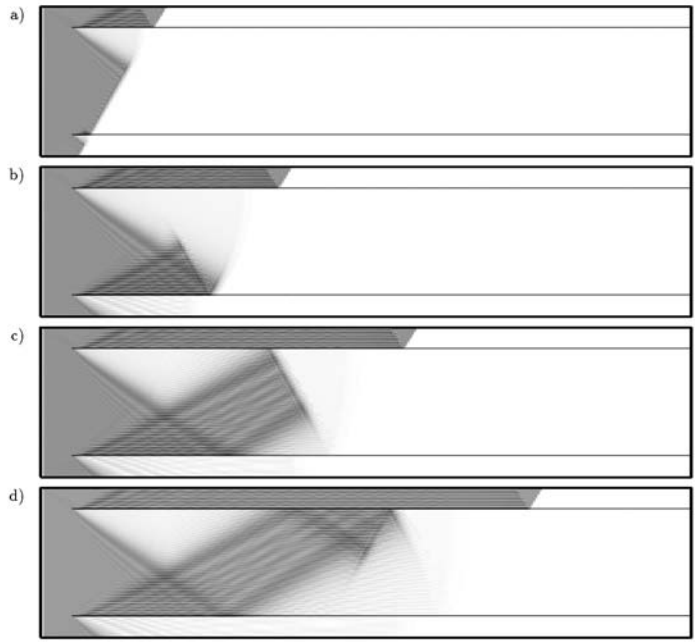


**Figure 13.** Shirai's and Felsen's open-ended waveguide problem: time-domain snapshots of the TE-polarized plane wave coupling into the waveguide, computed with the 2D-TE-EMFIT/2D-AFIT code.

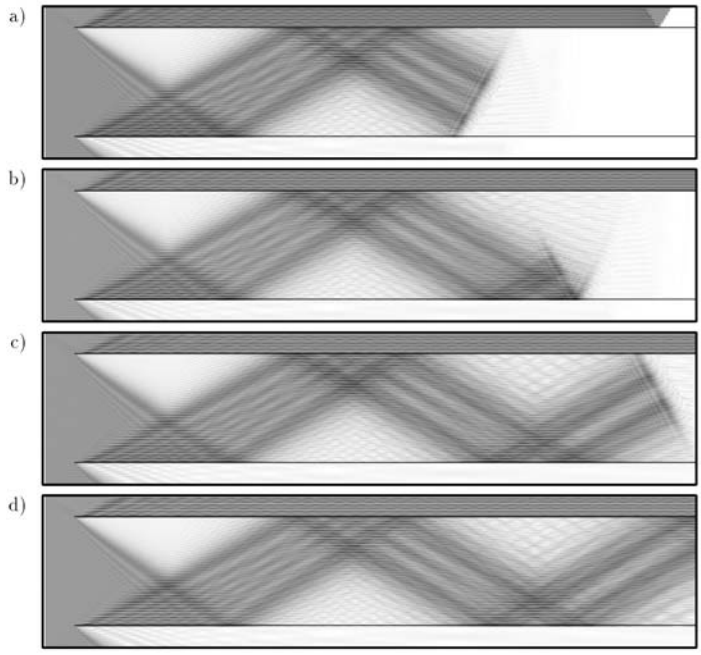


**Figure 14.** Shirai's and Felsen's open-ended waveguide problem: time-domain snapshots of the TE-polarized plane wave coupling into the waveguide, computed with the two-dimensional TE-EMFIT/2D-AFIT code.

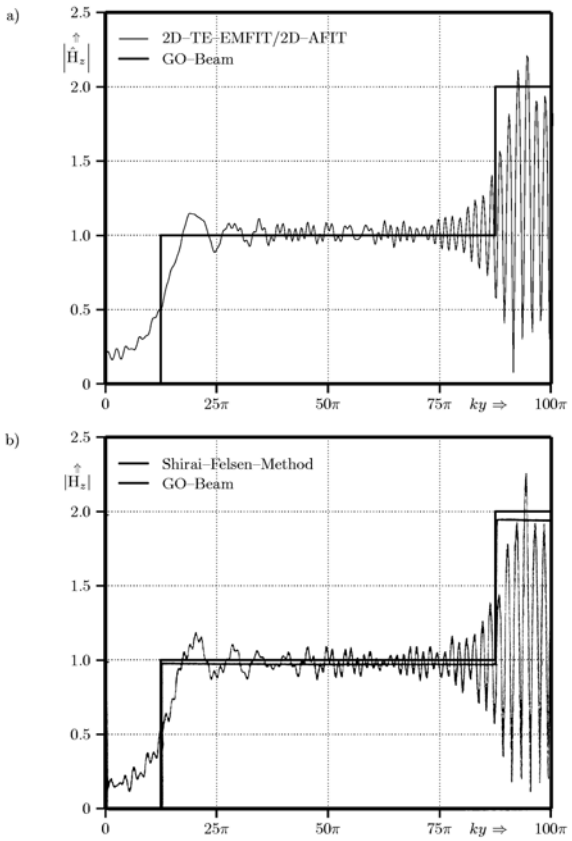


**Figure 15.** Shirai's and Felsen's open-ended waveguide problem: validation of the cross-section computed with the 2D-TE-EMFIT/2D-AFIT (top) against the cross section computed by *Shirai and Felsen* [1987] (bottom) at $kx = 68$ from the opening of the waveguide. Note that a second GO beam appears in Figure 15b. This is because the GO beam in the original publication was a bit shifted.

### 3.3.3 Volume and Surface Line-Source Excitation of an Isotropic Solid Steel Block with EFIT

Figure 16 shows two-dimensional EFIT results for the excitation of an isotropic solid steel block by a volume and surface line source. The time history of the broadband excitation pulse is given at the top of Figure 16. In Figure 16a, a vertically oriented line force excites cylindrical primary and secondary wave fields. Figure 16b shows Lamb's problem, where the source is located at a stress-free surface. The primary and secondary wave fields are connected by head waves traveling with the speed of the secondary wave and, additionally, Rayleigh surface waves, with a slightly lower velocity than the secondary wave, are supported. Of course, these numerical results can be validated against the analytical solutions.

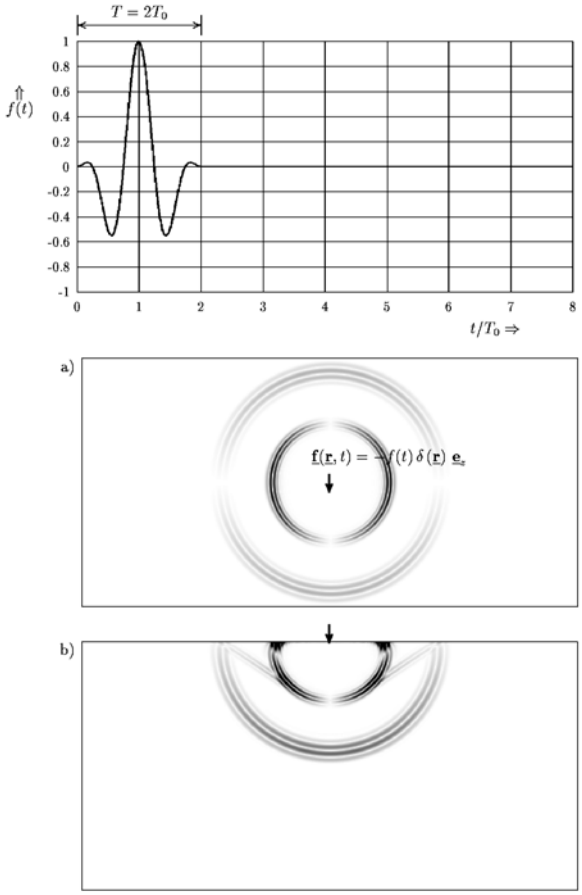


**Figure 16.** Time-domain 2D-P-SV-EFIT modeling results in the two-dimensional case, obtained for a broadband impulse displayed at the top: a) Impulsive elastodynamic wave fields excited by a vertically oriented line force radiating into an isotropic solid material; b) Impulsive wave field excited by a vertically oriented line force into a homogeneous isotropic solid half-space.

### 3.3.4 Ultrasonic Transducer (Antenna) Modeling with EFIT

Figure 17 displays two-dimensional EFIT modeling results for different types of ultrasonic antennas (transducers), which are typically applied in nondestructive testing. The extension of the vertically oriented line force of Lamb's problem in Figure 16b to a uniformly distributed, vertically orientated strip force in Figure 17a excites a dominant longitudinal plane wave – which is mainly used in the application – plus cylindrical pressure and shear vertical waves from both edges, as well as head waves and Rayleigh surface waves. If a linear delay is introduced into the driving force, different types of ultrasonic transducers can be modeled, as shown in Figures 17b-f. For instance, Figure 17e displays a shear 45º wave transducer, which is typically applied to the NDT situation in Figure 2, and generates an output as displayed in the plot shown in Figure 3.

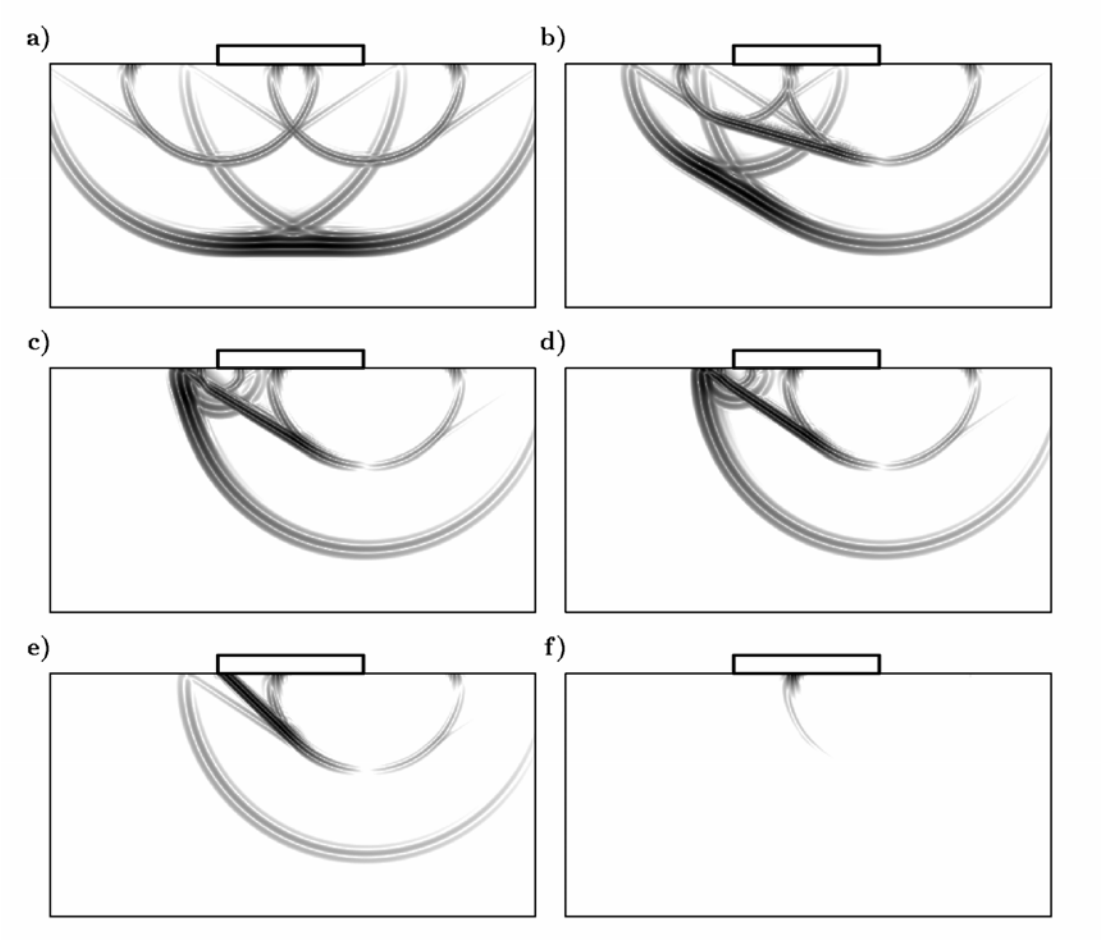


**Figure 17.** Time-domain EFIT ultrasonic transducer modeling in the two-dimensional pressure-shear vertical (P-SV) case: a) longitudinal 0° wave transducer; b) longitudinal 30° wave transducer; c) longitudinal 70° wave transducer; d) subsurface longitudinal wave transducer; e) shear 45° wave transducer; f) Rayleigh wave transducer.

## 4. COUPLED WAVE FIELDS: PIEZOELECTRIC AND ELECTROMAGNETIC-ULTRASONIC WAVE FIELDS

This section presents a unified formulation of coupled electromagnetic-acoustic-elastodynamic wave-field phenomena [*Nelson*, *1979*; *Auld*, *1990*; *Lerch*, *1990*; *Dai and Ludwig*, *1990*; *Roberts*, *1991*; *Ludwig and Dai*, *1991*; *Thompson*, *1993*, *Campbell*, *1998*; *Hashimoto*, *2000*; *Royer and Dieulesaint*, *2000a*, *b*], which occur in many applications. Examples include surface-acoustic-wave devices, applied in mobile and wireless communications, and piezoelectric and electromagnetic-ultrasonic antennas, as sketched in Figure 18, which are called ultrasonic transducers. Both types of antennas are applied to various applications, for instance, in non-destructive testing and medical diagnosis with ultrasound. The typical frequency range and spatial dimensions of both transducer types allow the introduction of low-frequency approximations into

the electromagnetic field equations. This means that in the piezoelectric case, we apply the electro-quasistatic (EQS) approximation, and in the electromagnetic-ultrasonic case, we use the magneto-quasistatic (MQS) approximation, respectively.

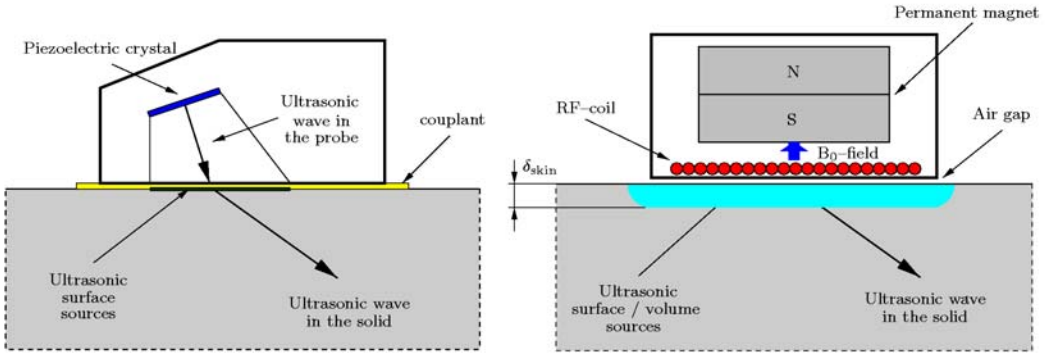


**Figure 18.** Different transducer types for exciting and receiving ultrasonic waves: a piezoelectric transducer (left) and an electromagnetic-ultrasonic (EMUS) transducer (right).

The governing equations for piezoelectric as well as electromagnetic-ultrasonic phenomena are the coupled equations for electromagnetic and elastic waves, given by Equations (3)-(6). Equations (3) and (4) are, in general, aided by the compatibility relations [*de Hoop*, *1995*]

$$\nabla \bullet \underline{\mathbf{B}}(\underline{\mathbf{R}},t) = \rho_{\mathrm{m}}(\underline{\mathbf{R}},t) \tag{50}$$

$$\nabla \bullet \underline{\mathbf{D}}(\underline{\mathbf{R}},t) = \rho_{\mathrm{e}}(\underline{\mathbf{R}},t)\,. \tag{51}$$

$\rho_{\mathrm{m}}(\underline{\mathbf{R}},t)$ [Vs/m$^3$] and $\rho_{\mathrm{e}}(\underline{\mathbf{R}},t)$ [As/m$^3$] are the magnetic and electric charge densities, and the magnetic and electric current and charge densities must fulfill the following continuity equations:

$$\nabla \bullet \underline{\mathbf{J}}_{\mathrm{m}}(\underline{\mathbf{R}},t) = -\frac{\partial}{\partial t}\rho_{\mathrm{m}}(\underline{\mathbf{R}},t) \tag{52}$$

$$\nabla \bullet \underline{\mathbf{J}}_{\mathrm{e}}(\underline{\mathbf{R}},t) = -\frac{\partial}{\partial t}\rho_{\mathrm{e}}(\underline{\mathbf{R}},t)\,. \tag{53}$$

From Equations (50) and (51), the following transition/continuity conditions are derived:

$$\underline{\mathbf{n}} \bullet \underline{\mathbf{B}}^{(2)}(\underline{\mathbf{R}},t) - \underline{\mathbf{n}} \bullet \underline{\mathbf{B}}^{(1)}(\underline{\mathbf{R}},t) = \begin{cases} \eta_{\mathrm{m}}(\underline{\mathbf{R}},t) & \text{with interface sources} \\ 0 & \text{source-free} \end{cases}, \tag{54}$$

$$\underline{\mathbf{n}} \bullet \underline{\mathbf{D}}^{(2)}(\underline{\mathbf{R}},t) - \underline{\mathbf{n}} \bullet \underline{\mathbf{D}}^{(1)}(\underline{\mathbf{R}},t) = \begin{cases} \eta_{\mathrm{e}}(\underline{\mathbf{R}},t) & \text{with interface sources} \\ 0 & \text{source-free} \end{cases}, \tag{55}$$

where $\eta_m(\underline{\mathbf{R}},t)$ [Vs/m$^2$] and $\eta_e(\underline{\mathbf{R}},t)$ [As/m$^2$] are the field-independent magnetic and electric surface charge densities. Note that boundary conditions are obtained via the same procedure as described above, where for a PEC boundary $\eta_e(\underline{\mathbf{R}},t)$ is a field-dependent source and $\eta_m(\underline{\mathbf{R}},t)$ vanishes.

### 4.1. PIEZOELECTRIC WAVE FIELDS

Piezoelectric waves, also called elasto-electric waves, rely on the following constitutive relations, which, for linear, homogeneous, anisotropic, instantaneously and locally reacting piezoelectric (pe) media [*Berlincourt et al.*, *1964*], read

$$\underline{\mathbf{D}}(\underline{\mathbf{R}},t) = \underline{\underline{\boldsymbol{\varepsilon}}}^{S}(\underline{\mathbf{R}}) \bullet \underline{\mathbf{E}}(\underline{\mathbf{R}},t) + \underline{\underline{\underline{\mathbf{e}}}}_{pe}(\underline{\mathbf{R}}) : \underline{\underline{\mathbf{S}}}(\underline{\mathbf{R}},t) \tag{56}$$

$$\underline{\underline{\mathbf{S}}}(\underline{\mathbf{R}},t) = [\underline{\underline{\underline{\mathbf{d}}}}_{pe}(\underline{\mathbf{R}})]^{231} \bullet \underline{\mathbf{E}}(\underline{\mathbf{R}},t) + \underline{\underline{\underline{\mathbf{s}}}}^{E}(\underline{\mathbf{R}}) : \underline{\underline{\mathbf{T}}}(\underline{\mathbf{R}},t)\,. \tag{57}$$

| | | | | | |
|---|---|---|---|---|---|
| $\underline{\underline{\boldsymbol{\varepsilon}}}^{S}$ | [As/Vm] | Permittivity tensor of 2nd rank (dyad) at $\underline{\mathbf{S}} = \text{const.}$ | $\underline{\underline{\underline{\mathbf{e}}}}_{pe}$ | As/m$^2$] | Piezoelectric coupling tensor of 3rd rank (triad) with $\underline{\underline{\underline{\mathbf{e}}}}_{pe} = \underline{\underline{\underline{\mathbf{d}}}}_{pe} : [\underline{\underline{\underline{\mathbf{s}}}}^{E}]^{-1}$ |
| $\underline{\underline{\underline{\mathbf{s}}}}^{E}$ | [m$^2$/N] | Compliance tensor of 4th rank (tetrad) at $\underline{\mathbf{E}} = \text{const.}$ | $\underline{\underline{\underline{\mathbf{d}}}}_{pe}$ | [As/N] | Piezoelectric coupling tensor of 3rd rank (triad) with $\underline{\underline{\underline{\mathbf{d}}}}_{pe} = \underline{\underline{\underline{\mathbf{e}}}}_{pe} : \underline{\underline{\underline{\mathbf{s}}}}^{E}$ |

The upper index notation "231" indicates the order of transposition of the unit vectors. A coordinate-free representation of the material tensors can be found in *Marklein* [*1997*].

#### 4.1.1 Electro-Quasistatic (EQS) Approximation

If we assume that the typical dimension of the piezoelectric material is small compared to the electromagnetic wavelength – the low-frequency approximation for Maxwell's equations – we can neglect the induction term in Faraday's law, $\frac{\partial}{\partial t}\underline{\mathbf{B}}(\underline{\mathbf{R}},t) = \underline{\mathbf{0}}$. This allows us to represent the electric field strength by an irrotational gradient field

$$\underline{\mathbf{E}}(\underline{\mathbf{R}},t) = -\nabla\Phi(\underline{\mathbf{R}},t)\,, \tag{58}$$

with the scalar electric potential $\Phi(\underline{\mathbf{R}},t)$ [V], where $\nabla \times \underline{\mathbf{E}}(\underline{\mathbf{R}},t) = \underline{\mathbf{0}}$ holds. This is the so-called electro-quasistatic (EQS) approximation [*Haus and Melcher*, *1989*]. Finally, with the EQS approximation of Equation (58), we find, from Equation (51), by computing the first-order time derivative and Equations (56) and (6), an elliptic Poisson equation for the first-order time derivative of the scalar electric potential:

$$\nabla \bullet \left[ \underline{\underline{\boldsymbol{\varepsilon}}}^{\mathrm{S}}(\underline{\mathbf{R}}) \bullet \nabla \frac{\partial}{\partial t} \Phi(\underline{\mathbf{R}}, t) \right] = \nabla \bullet \underline{\underline{\mathbf{e}}}_{\mathrm{pe}}(\underline{\mathbf{R}}) : \mathrm{sym}\{\nabla \underline{\mathbf{v}}(\underline{\mathbf{R}}, \mathrm{t})\} - \frac{\partial}{\partial t} \rho_{\mathrm{e}}(\underline{\mathbf{R}}, t) , \tag{59}$$

where we assumed $\underline{\underline{\mathbf{h}}}(\underline{\mathbf{R}}, t) = \underline{\underline{\mathbf{0}}}$ for the source term in Equation (6).

### 4.1.2 Piezoelectric Finite Integration Technique (PFIT)

Applying the Finite Integration Technique to the integral form of Equation (59) and the governing equations of elastodynamics, using a dual-grid complex as shown in Figure 19, we obtain the following set of piezoelectric grid equations in matrix form for the so-called current-driven PFIT algorithm [*Marklein*, *1997*]:

$$\{\dot{\mathbf{v}}\}^{(n_t - 1/2)} = [\tilde{\boldsymbol{\rho}}_{\mathrm{p0}}]^{-1} [\widetilde{\mathbf{DIV}}] [\widetilde{\mathbf{R}}_{\dot{\mathrm{v}}}^{\mathrm{T}}] [\mathbf{A}_{\dot{\mathrm{v}}}^{\mathrm{T}}] \{\mathbf{T}\}^{(n_t - 1/2)} + [\tilde{\boldsymbol{\rho}}_{\mathrm{p0}}]^{-1} \{\mathbf{f}\}^{(n_t - 1/2)} \tag{60}$$

$$\{\mathbf{v}\}^{(n_t)} = \{\mathbf{v}\}^{(n_t - 1)} + \Delta t \{\dot{\mathbf{v}}\}^{(n_t - 1/2)} \tag{61}$$

$$\begin{aligned} [\widetilde{\mathbf{div}}][\tilde{\mathbf{S}}]][\tilde{\boldsymbol{\varepsilon}}^{\mathrm{S}}][\mathbf{R}]^{-1}[\mathbf{grad}]\{\dot{\boldsymbol{\Phi}}\}^{(n_t)} = {} & [\widetilde{\mathbf{div}}][\tilde{\mathbf{S}}][\tilde{\mathbf{e}}_{\mathrm{pe}}][\mathbf{R}_{\dot{\Phi}}^{\mathrm{v}}]^{-1}[\mathbf{GRad}][\mathbf{A}_{\dot{\Phi}}^{\mathrm{v}}]\{\mathbf{v}\}^{(n_t)} \\ & - [\mathbf{V}_{\dot{\Phi}}^{\dot{\rho}}]\{\dot{\boldsymbol{\rho}}_{\mathrm{e}}\}^{(n_t)} - [\mathbf{S}_{\dot{\Phi}}^{\dot{\eta}}]\{\dot{\boldsymbol{\eta}}_{\mathrm{e}}\}^{(n_t)} \end{aligned} \tag{62}$$

$$\{\dot{\mathbf{T}}\}^{(n_t)} = [\mathbf{c}^{\mathrm{E}}][\mathbf{R}_{\dot{\mathrm{T}}}^{\mathrm{v}}]^{-1}[\mathbf{GRAD}][\mathbf{A}_{\dot{\mathrm{T}}}^{\mathrm{v}}]\{\mathbf{v}\}^{(n_t)} + [\mathbf{e}_{\mathrm{pe}}^{21}][\mathbf{R}_{\dot{\mathrm{T}}}^{\Phi}]^{-1}[\mathbf{A}_{\dot{\mathrm{T}}}^{\dot{\Phi}}][\mathbf{grad}]\{\dot{\boldsymbol{\Phi}}\}^{(z)} + \{\mathbf{g}\}^{(z)} \tag{63}$$

$$\{\mathbf{T}\}^{(n_t + 1/2)} = \{\mathbf{T}\}^{(n_t - 1/2)} + \Delta t \{\dot{\mathbf{T}}\}^{(n_t)} \tag{64}$$

with $[\mathbf{curl}]\{\mathbf{E}\}^{(n_t)} = \{\mathbf{0}\}$ and $\{\mathbf{E}\}^{(n_t)} = -[\mathbf{R}]^{-1}[\mathbf{grad}]\{\boldsymbol{\Phi}\}^{(n_t)}$. In the above matrix equations $\{\boldsymbol{\Phi}\}$, $\{\boldsymbol{\rho}_{\mathrm{e}}\}$, $\{\boldsymbol{\eta}_{\mathrm{e}}\}$, and $\{\mathbf{E}\}$ are additional algebraic field vectors; $[\tilde{\boldsymbol{\rho}}_{\mathrm{p0}}]$, $[\tilde{\boldsymbol{\varepsilon}}^{\mathrm{S}}]$, $[\tilde{\mathbf{e}}_{\mathrm{pe}}]$, and $[\mathbf{e}_{\mathrm{pe}}^{21}]$ are additional material matrices; $[\mathbf{R}_{\dot{\Phi}}^{\mathrm{v}}]$, $[\mathbf{R}_{\dot{\mathrm{T}}}^{\dot{\Phi}}]$, $[\mathbf{S}]$, $[\tilde{\mathbf{S}}]$, $[\mathbf{S}_{\dot{\Phi}}^{\dot{\eta}}]$, and $[\mathbf{V}_{\dot{\Phi}}^{\dot{\rho}}]$ are additional matrices

containing the finite distances, surfaces, and volumes, and $[\mathbf{A}_{\dot{\Phi}}^{\mathrm{v}}]$ and $[\mathbf{A}_{\dot{\mathrm{T}}}^{\dot{\Phi}}]$ are additional averaging matrices. The matrix operator $[\mathbf{GRad}]$ is an additional topological operator, which contains only the integer numbers $\{-1, 0, 1\}$.

In general, the PFIT comes in two versions, a voltage-driven and a current-driven version. The latter is usually combined with a one-dimensional network algorithm in order to take into account an impedance load. In fact, the PFIT is a coupled explicit elliptic-hyperbolic marching-on-in-time solver of the leapfrog type. For the solution of the elliptic part of the algorithm, standard techniques, like a conjugate-gradient (CG) type of algorithm, can be applied. Details and results can be found in *Marklein* [*1997*, *2000a*, *b*], *Marklein and Glitza* [*1997*], *Marklein et al*. [*1998*, *1999*], *Marklein and Langenberg* [*1998*], and *Langenberg et al.* [*2002*]. For the finite-element modeling of piezoelectric wave fields, see, for example, *Lerch* [*1990*] and *Roberts* [*1991*].

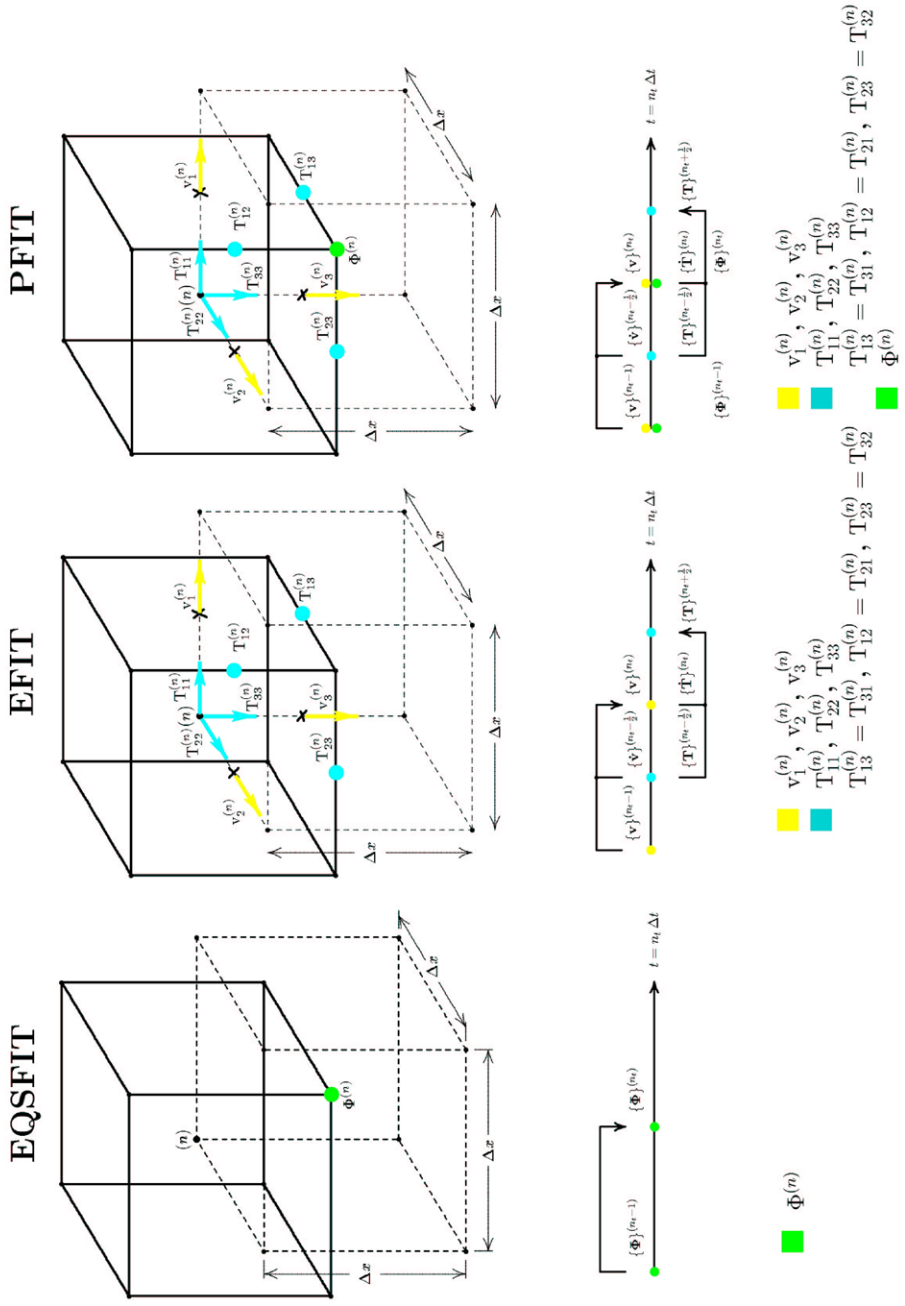


**Figure 19.** The spatial and temporal grid complex of EQSFIT, EFIT, and PFIT, and the allocation of the local discrete field quantities (also see Plate 3).

### 4.2 ELECTROMAGNETIC-ULTRASONIC WAVE FIELDS

There are two different ways to excite ultrasonic waves in an electrically conducting solid material: either a Lorentz force distribution is excited or, if applicative, we make use of the piezo-magnetic effect (biased magnetostrictive case). In the first case, a (magnetic) Lorentz volume force density, according to

$$\underline{\mathbf{f}}(\underline{\mathbf{R}},t) = \underline{\mathbf{f}}_{\mathrm{m}}(\underline{\mathbf{R}},t) = \underline{\mathbf{J}}_{\mathrm{eed}}(\underline{\mathbf{R}},t) \times \underline{\mathbf{B}}_0(\underline{\mathbf{R}}) \tag{65}$$

is generated, where $\underline{\mathbf{B}}_0(\underline{\mathbf{R}})$ is a static magnetic flux density, in general generated by a permanent-magnet configuration. $\underline{\mathbf{J}}_{\mathrm{eed}}(\underline{\mathbf{R}},t)$ is a transient electric eddy-current density (these flow in closed paths), given by Ohm's law for a material at rest (approximation)

$$\underline{\mathbf{J}}_{\mathrm{eed}}(\underline{\mathbf{R}},t) = \underline{\mathbf{J}}_{\mathrm{e}\sigma\mathrm{E}}(\underline{\mathbf{R}},t) = \underline{\underline{\boldsymbol{\sigma}}}(\underline{\mathbf{R}}) \bullet \underline{\mathbf{E}}(\underline{\mathbf{R}},t)\,, \tag{66}$$

with the tensorial electric conductivity $\underline{\underline{\boldsymbol{\sigma}}}$ [A/Vm].

The properties of a linear, inhomogeneous, anisotropic, instantaneously and locally reacting piezo-magnetic (pm) media (also the biased magnetostrictive case) are given by the following constitutive relations [*Berlincourt et al.*, *1964*]:

$$\underline{\mathbf{B}}(\underline{\mathbf{R}},t) = \underline{\underline{\boldsymbol{\mu}}}^{\mathrm{S}}(\underline{\mathbf{R}}) \bullet \underline{\mathbf{H}}(\underline{\mathbf{R}},t) + \underline{\underline{\underline{\mathbf{e}}}}_{\mathrm{pm}}(\underline{\mathbf{R}}) : \underline{\underline{\mathbf{S}}}(\underline{\mathbf{R}},t) \tag{67}$$

$$\underline{\underline{\mathbf{S}}}(\underline{\mathbf{R}},t) = [\underline{\underline{\underline{\mathbf{d}}}}_{\mathrm{pm}}(\underline{\mathbf{R}})]^{231} \bullet \underline{\mathbf{H}}(\underline{\mathbf{R}},t) + \underline{\underline{\underline{\mathbf{s}}}}^{\mathrm{H}}(\underline{\mathbf{R}}) : \underline{\underline{\mathbf{T}}}(\underline{\mathbf{R}},t)\,. \tag{68}$$

| | | | | | |
|---|---|---|---|---|---|
| $\underline{\underline{\boldsymbol{\mu}}}^{\mathrm{S}}$ | [Vs/Am] | Permeability tensor of 2nd rank (dyad) at $\underline{\mathbf{S}} = \text{const.}$ | $\underline{\underline{\underline{\mathbf{e}}}}_{\mathrm{pm}}$ | [Vs/m$^2$] | Piezomagnetic coupling tensor of 3rd rank (triad) with $\underline{\underline{\underline{\mathbf{e}}}}_{\mathrm{pm}} = \underline{\underline{\underline{\mathbf{d}}}}_{\mathrm{pm}} : [\underline{\underline{\underline{\mathbf{s}}}}^{\mathrm{H}}]^{-1}$ |
| $\underline{\underline{\underline{\mathbf{s}}}}^{\mathrm{H}}$ | [m$^2$/N] | Compliance tensor of 4th rank (tetrad) at $\underline{\mathbf{H}} = \text{const.}$ | $\underline{\underline{\underline{\mathbf{d}}}}_{\mathrm{pm}}$ | [Vs/N] | Piezomagnetic coupling tensor of 3rd rank (triad) with $\underline{\underline{\underline{\mathbf{d}}}}_{\mathrm{pm}} = \underline{\underline{\underline{\mathbf{e}}}}_{\mathrm{pm}} : \underline{\underline{\underline{\mathbf{s}}}}^{\mathrm{H}}$ |

In the reception mode, we take into account the effect of a moving electrically conducting material within the low-velocity approximation [*Landau et al.*, *1984*]. Then, Ohm's law in Equation (66) reads

$$\underline{\mathbf{J}}_{\mathrm{eed}}(\underline{\mathbf{R}},t) = \underbrace{\underline{\underline{\boldsymbol{\sigma}}}(\underline{\mathbf{R}}) \bullet \underline{\mathbf{E}}(\underline{\mathbf{R}},t)}_{\underline{\mathbf{J}}_{\mathrm{e}\sigma\,\mathrm{E}}(\underline{\mathbf{R}},t)} + \underbrace{\underline{\underline{\boldsymbol{\sigma}}}(\underline{\mathbf{R}}) \bullet \left[\underline{\mathbf{v}}(\underline{\mathbf{R}},t) \times \underline{\mathbf{B}}_0(\underline{\mathbf{R}})\right]}_{\underline{\mathbf{J}}_{\mathrm{e}\sigma\mathrm{v}\mathrm{B}_0}(\underline{\mathbf{R}},t)}\,. \tag{69}$$

#### 4.2.1 Magneto-Quasistatic (MQS) Approximation

If the typical dimension of the piezo-magnetic material is small compared to the electromagnetic wavelength – the low-frequency approximation for Maxwell's equations – we can

neglect the displacement current in the Ampère-Maxwell circuital law, i.e., $\frac{\partial}{\partial t}\underline{\mathbf{D}}(\underline{\mathbf{R}},t)=\underline{\mathbf{0}}$. Further, let $\{\boldsymbol{\rho}_{\mathrm{m}}\}=\{\mathbf{0}\}$. Then, the magnetic flux density, $\underline{\mathbf{B}}(\underline{\mathbf{R}},t)$, is a solenoidal field, which can be represented as the curl of the magnetic vector potential $\underline{\mathbf{A}}(\underline{\mathbf{R}},t)$ [Vs/m], i.e., $\underline{\mathbf{B}}(\underline{\mathbf{R}},t)=\nabla\times\underline{\mathbf{A}}(\underline{\mathbf{R}},t)$, where $\nabla\bullet\underline{\mathbf{A}}(\underline{\mathbf{R}},t)=0$ must hold. Then, the electric field strength is given by

$$\underline{\mathbf{E}}(\underline{\mathbf{R}},t)=-\frac{\partial}{\partial t}\underline{\mathbf{A}}(\underline{\mathbf{R}},t)\,. \tag{70}$$

This is the magneto-quasistatic (MQS) approximation, which results in a parabolic diffusion equation for the magnetic vector potential. With $\underline{\underline{\boldsymbol{\nu}}}^{\mathrm{S}}=(\underline{\underline{\boldsymbol{\mu}}}^{\mathrm{S}})^{-1}$, this reads

$$\nabla\times\left[\underline{\underline{\boldsymbol{\nu}}}^{\mathrm{S}}(\underline{\mathbf{R}})\bullet\nabla\times\underline{\mathbf{A}}(\underline{\mathbf{R}},t)\right]+\underline{\underline{\boldsymbol{\sigma}}}(\underline{\mathbf{R}})\bullet\frac{\partial}{\partial t}\underline{\mathbf{A}}(\underline{\mathbf{R}},t)=\underline{\mathbf{J}}_{\mathrm{ei}}(\underline{\mathbf{R}},t)+\underline{\underline{\boldsymbol{\sigma}}}(\underline{\mathbf{R}})\bullet\left[\underline{\mathbf{v}}(\underline{\mathbf{R}},t)\times\underline{\mathbf{B}}_0(\underline{\mathbf{R}})\right], \tag{71}$$

where the electric current density is $\underline{\mathbf{J}}_{\mathrm{e}}(\underline{\mathbf{R}},t)=\underline{\mathbf{J}}_{\mathrm{ei}}(\underline{\mathbf{R}},t)+\underline{\mathbf{J}}_{\mathrm{e}\sigma\mathrm{E}}(\underline{\mathbf{R}},t)+\underline{\mathbf{J}}_{\mathrm{e}\sigma\mathrm{v}\mathrm{B}_0}(\underline{\mathbf{R}},t)$. In the excitation mode, Equation (71) is driven by $\underline{\mathbf{J}}_{\mathrm{ei}}(\underline{\mathbf{R}},t)$ as the impressed electric current density in the RF coil, while $\underline{\mathbf{J}}_{\mathrm{e}\sigma\mathrm{v}\mathrm{B}_0}(\underline{\mathbf{R}},t)$ is usually neglected in the excitation mode. In the reception mode, the driving term is given by $\underline{\mathbf{J}}_{\mathrm{e}\sigma\mathrm{v}\mathrm{B}_0}(\underline{\mathbf{R}},t)$, while $\underline{\mathbf{J}}_{\mathrm{ei}}(\underline{\mathbf{R}},t)$ is assumed to be zero.

### 4.2.2 Electromagnetic-Ultrasonic Finite Integration Technique (EMUSFIT)

Applying the Finite Integration Technique to the integral form of Equation (71) and the governing equations of elastodynamics, using the dual-grid complex as given in Figure 20, yields the grid equations of the electromagnetic-ultrasonic FIT (EMUSFIT) in matrix form. In particular, if we neglect the outer right term in Equation (71), the discrete form of Equation (71) in integral form reads

$$[\widetilde{\mathbf{R}}][\widetilde{\mathbf{curl}}][\tilde{\mathbf{v}}^{\mathrm{S}}][\mathbf{R}]^{-1}[\mathbf{curl}]\{\mathbf{A}\}^{(n_t+1)}+[\tilde{\mathbf{S}}][\tilde{\boldsymbol{\sigma}}]\{\dot{\mathbf{A}}\}^{(n_t+1)}=[\tilde{\mathbf{S}}]\{\mathbf{J}_{\mathrm{ei}}\}^{(n_t+1)}+[\tilde{\mathbf{S}}][\tilde{\boldsymbol{\sigma}}]\{\mathbf{v}\times\mathbf{B}_0\}^{(n_t+1)} \tag{72}$$

with the property $[\widetilde{\mathbf{div}}]\{\mathbf{A}\}^{(n_t+1)}=\{\mathbf{0}\}$. In the above matrix equations $\{\mathbf{A}\}$, $\{\mathbf{J}_{\mathrm{ei}}\}$, $\{\mathbf{v}\times\mathbf{B}_0\}$ are additional algebraic field vectors and $[\tilde{\mathbf{v}}^{\mathrm{S}}]$ and $[\boldsymbol{\sigma}]$ are additional material matrices.

Introducing a first-order backward finite-difference approximation in time in Equation (72), the MQSFIT grid equation can be written in standard matrix form $[\mathbf{A}]\{\mathbf{x}\}=\{\mathbf{b}\}$, which can be solved with a standard algorithm, like a conjugate-gradient (CG) algorithm. A comprehensive study of other solution methods can be found in *Clemens* [*1998*], *Clemens and Weiland* [*1999*,

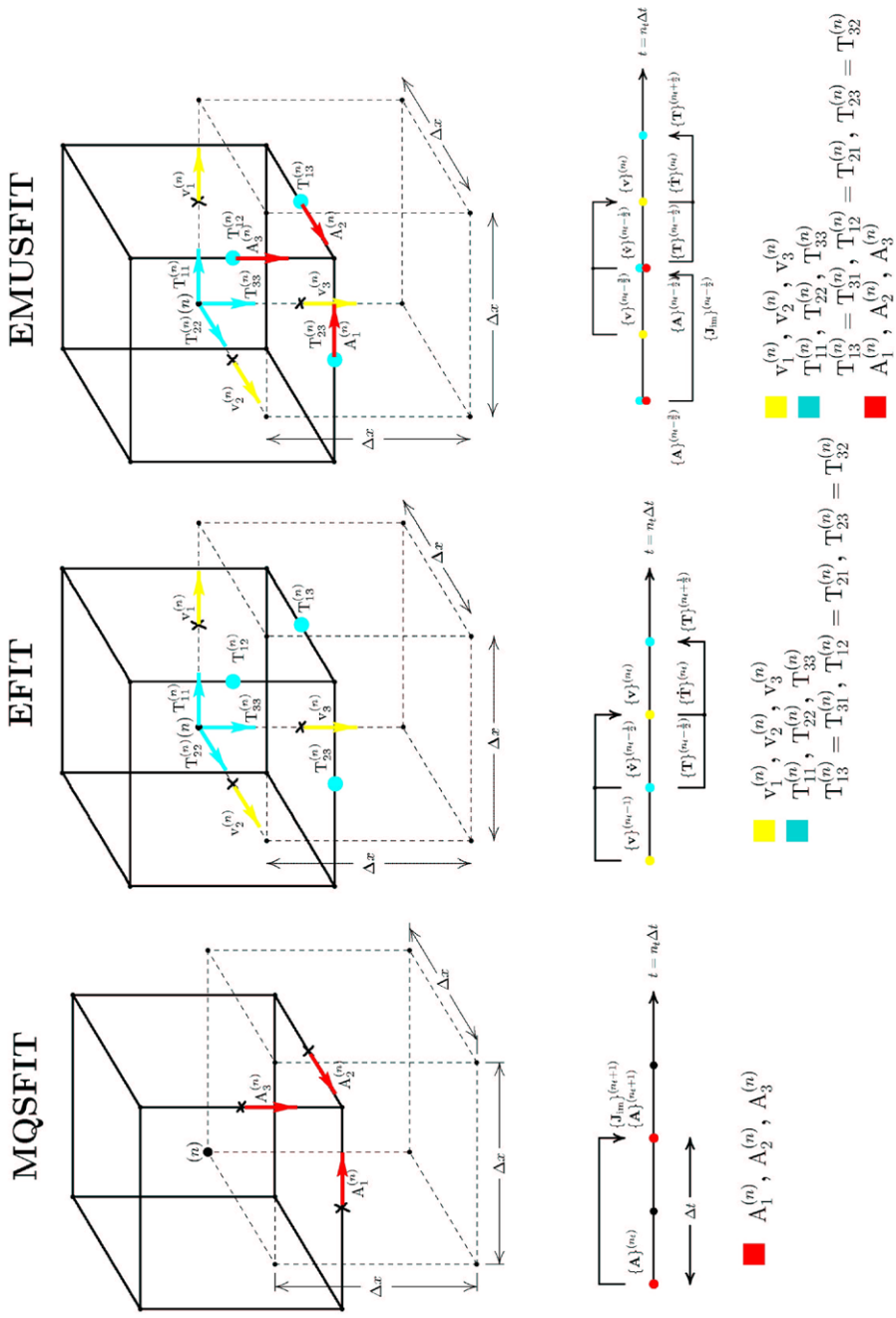


**Figure 20.** The spatial and temporal grid complex of MQSFIT, EFIT, and EMUSFIT, and the allocation of the local discrete field quantities (see also Plate 4).

*2001*], and *Clemens et al.* [*2001*]. In total, EMUSFIT is a mixed explicit elliptic-parabolic-hyperbolic marching-on-in-time solver, consisting of an elliptic magnetostatic (MS) solver (MSFIT), a parabolic magneto-quasistatic (MQS) solver (MQSFIT), and the hyperbolic EFIT solver. The MSFIT is used to compute the magnetostatic field generated by a permanent magnet configuration as shown on the right of Figure 18.

In the excitation mode, Equation (72) is solved for the magnetic vector potential $\{\mathbf{A}\}^{(n_t+1)}$. From that we compute the electric field strength via Equation (70), and the so-called eddy current density via Equation (66). With a superimposed magnetostatic field, a resulting Lorentz force via Equation (65) excites an elastodynamic wave field. In the reception mode, according to Equation (69), the driving term in Equation (72) is the electric eddy current "induced" by the incident elastodynamic wave field. Then, the resulting vector potential from Equation (72) and the electric field strength from Equation (70) determine the induced electric voltage in the RF coil (see the right-hand side of Figure 18).

Note that the counterpart of the time-independent version of Equations (50) and (51) reads

$$[\mathbf{div}]\{\mathbf{B}\} = \{\boldsymbol{\rho}_\mathrm{m}\} \tag{73}$$

$$[\widetilde{\mathbf{div}}]\{\mathbf{D}\} = \{\boldsymbol{\rho}_\mathrm{e}\}\,, \tag{74}$$

where $\{\mathbf{D}\}$ and $\{\boldsymbol{\rho}_\mathrm{m}\}$ are additional algebraic field vectors, and $[\widetilde{\mathbf{div}}]$ is an additional algebraic topological operator, which contain only the integers $\{-1,0,1\}$.

This makes it clear that the Finite Integration Technique (FIT) can also be applied to electrostatic and magnetostatic field problems as well, as pointed out by *Weiland* [*1996*]. For instance, Equation (73) is used for $\{\boldsymbol{\rho}_\mathrm{m}\} = \{\mathbf{0}\}$ (and $\{\mathbf{J}_\mathrm{m}\} = \{\mathbf{0}\}$) to compute the magnetostatic flux density $\{\mathbf{B}_0\}$ generated by a permanent magnet based on a scalar magnetic potential approach, where inside the permanent magnet an impressed magnetization is assumed. For the finite-element modeling of an electromagnetic-ultrasonic transducer see, for example, *Dai and Ludwig* [*1990*] and *Ludwig and Dai* [*1991*].

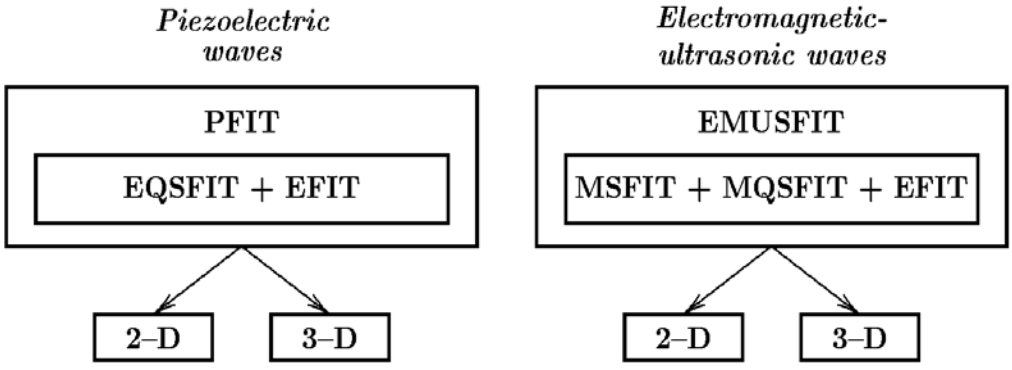


**Figure 21.** The PFIT (left) as a combination of the EQSFIT and EFIT, and the EMUSFIT (right) as a combination of the MSFIT, MQSFIT, and EFIT.

Figure 21 summarizes both algorithms: Essentially, the PFIT is a combination of the elliptic EQSFIT solver and the hyperbolic EFIT solver, and the EMUSFIT is a subsequent combination of the elliptic MSFIT solver for the magnetostatic flux density $\underline{\mathbf{B}}_0(\underline{\mathbf{R}})$, generated by a permanent-magnetic configuration, and the coupled parabolic MQSFIT solver, for the magnetic vector potential, and the hyperbolic EFIT solver for the ultrasonic wave propagation. Numerical results are presented in *Marklein et al.* [*1999*] and *Marklein* [*2000a*, *b*].

### 4.3 NUMERICAL EXAMPLES

#### 4.3.1 Piezoelectric Disk Transducer Modeling with PFIT

Figure 22 shows the modeling of a piezoelectric transducer coupled to a solid brass cylinder with a back-wall-breaking crack. The comparison between the modeled and experimental piezoelectric voltage observed at the piezoelectric disk given in Figure 22 shows an agreement between the numerical and physical world. The dominant echo signals are the excitation pulse (EP), the notch echo (NE), and the first back-wall echo (BE1). Time-domain snapshots of the particle velocity vector are displayed in Figure 23 showing the ultrasonic wave propagation and the generation of the so-called notch echo signal and back-wall echo signal.

#### 4.3.2 Electromagnetic-Ultrasonic Transducer Modeling with EMUSFIT

Figure 24 displays the numerical modeling of the excitation of a shear horizontal (SH) plate wave excited by an electromagnetic-ultrasonic transducer. The relatively long elastic waveguide is displayed in a stack of two subfigures. This transducer type generates a bi-directional wave field, a dispersion-free plane SH wave followed by higher order SH modes, as shown in the middle of Figure 24. The wave field is absorbed at both ends by an absorbing boundary condition. The SH wave field, which travels to the right, hits the surface breaking crack and is reflected back to the transducer. A comparison between the numerical result and experimental measurement is given at the bottom of Figure 24 reflecting the validation of the simulated echo signals.

## 5. CONCLUSIONS

This article reviewed the application of the Finite Integration Technique in acoustics, electromagnetics, elastodynamic, and coupled-wave-field problems, such as piezoelectric waves and electromagnetic-ultrasonic waves. In particular, this review tried to present the topic under consideration in a unified way, starting from the sets of field equations, constitutive relations, and transition/continuity as well as boundary conditions, up to the sets of discrete grid equations. This unified presentation will give a deep insight into the physical similarities between the different phenomena and their numerical treatment.

Due to the limited space and the various wave-field phenomena, it was impossible to cover all features of the Finite Integration Technique and its application to the time-domain computation of wave fields. The author hopes that this review paper will be informative to a broad audience, and will give the reader an overview of the Finite Integration Technique (FIT) applied to simulate wave fields of different kinds, and of the developed tools, which are applicable for the numerical solution of uncoupled/coupled field problems. In fact, the computation of coupled-field problems

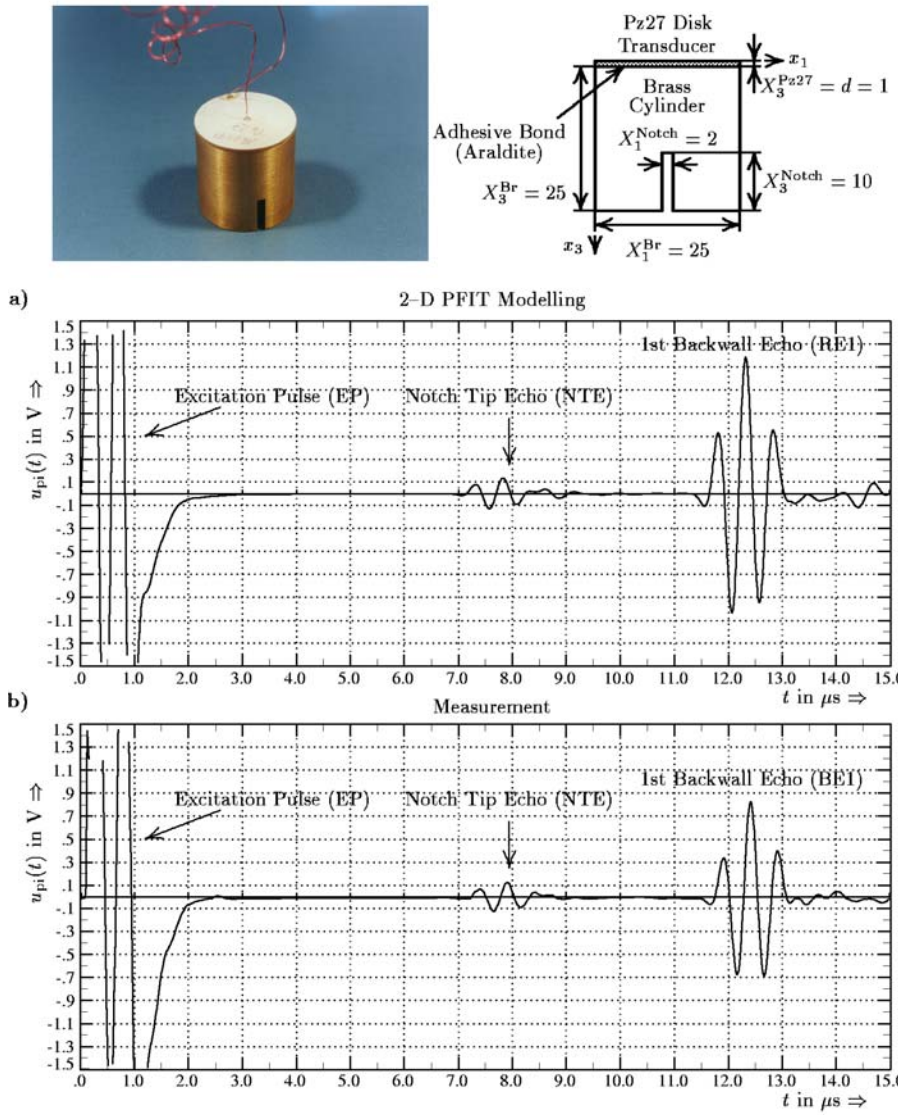


**Figure 22.** An ultrasonic piezoelectric Pz27 disk transducer on a brass cylinder with a back-wall-breaking notch. A photograph and the two-dimensional geometry for the two-dimensional PFIT modeling are given at the top. In the middle and the bottom figures a comparison between the computational result (a) and the experimental signal (b) is shown. The electric voltage response, $u_{pi}$, at the Pz27 disk (A-scan) for a resistive load of $R_g = 50\,\Omega$ and a sine-pulse excitation, with $u_0 = 10\,V$, $n = 2$ cycles, and $f_c = 2\,MHz$ is displayed. EP: excitation pulse; NTE: notch tip echo; BE1: first back-wall echo.

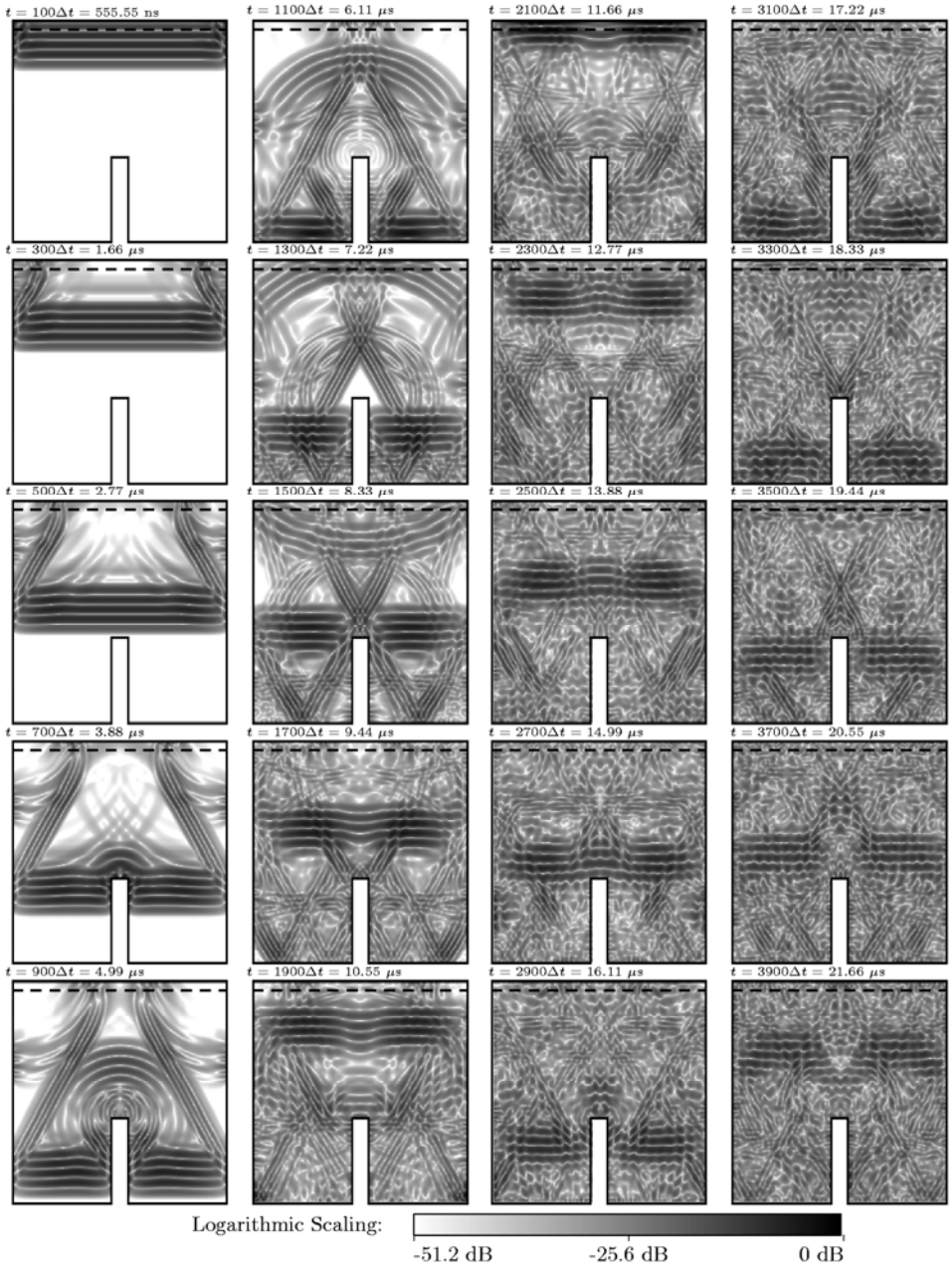


**Figure 23.** An ultrasonic piezoelectric Pz27 disk transducer on a solid brass cylinder with a back-wall-breaking notch: time-domain wave field snapshots of the two-dimensional PFIT modeling.

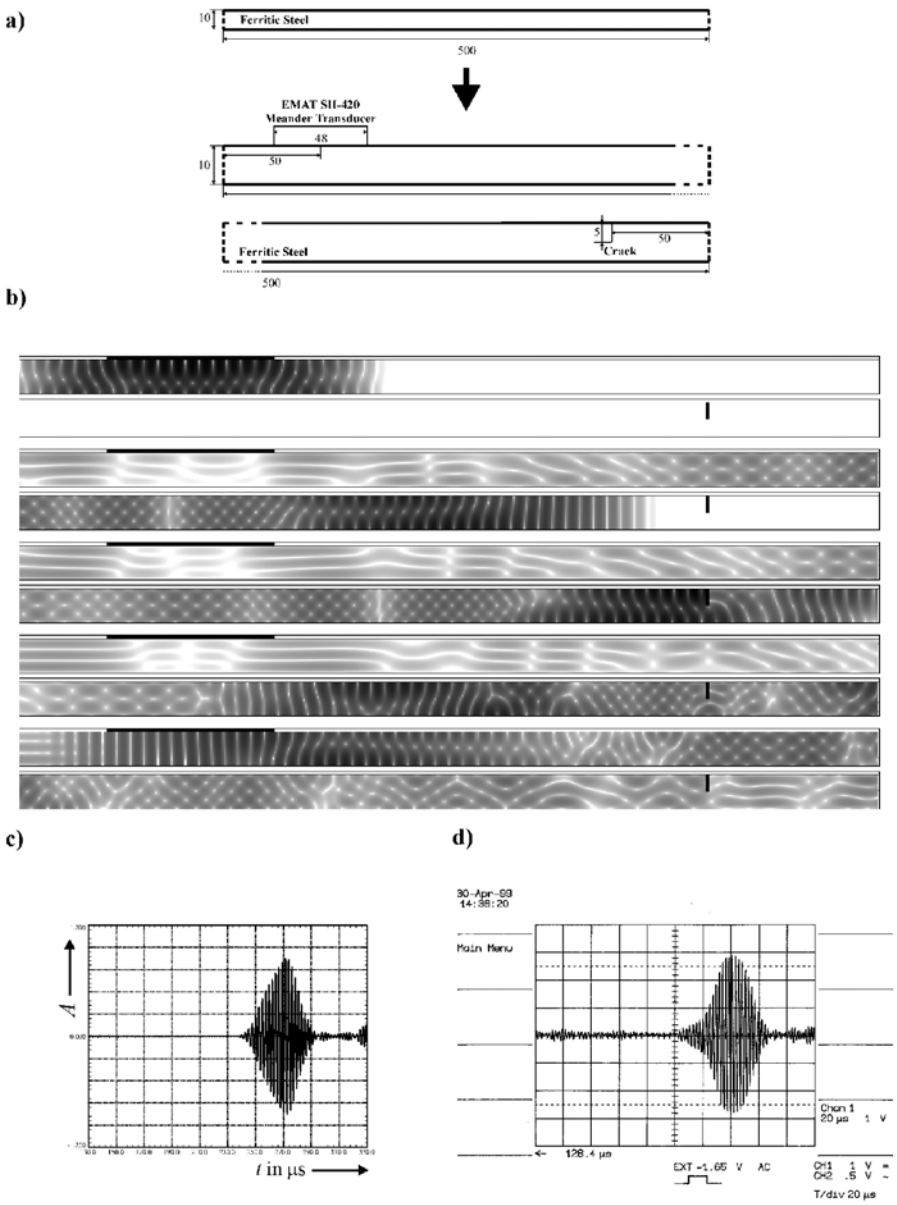


**Figure 24.** Time-domain EMUSFIT modeling results in the two-dimensional case. (a) The geometry of the solid plate – waveguide – with transducer and surface-breaking crack. (b) Two-dimensional SH-EMUSFIT time-domain snapshots. (c) and (d) display a comparison of the modeled and measured echo signals received in pulse-echo mode. (The measured A-scan is courtesy of G. Hübschen, Fraunhofer Institute for Nondestructive Testing, Germany.)

is increasingly needed for studying interdisciplinary wave-field effects in science and engineering, as well as related disciplines.

## 6. REFERENCES

J. D. Achenbach [1984], *Wave Propagation in Elastic Solid*, Amsterdam, North-Holland.

B. A. Auld [1990], *Acoustic Fields and Waves in Solids, Second Edition*, Malabar, R. E. Krieger Publishing Company.

M. Bartsch, M. Dehler, M. Dohlus, F. Ebeling, P. Hahne, R. Klatt, F. Krawczyk, M. Marx, Z. Min, T. Pröpper, D. Schmitt, P. Schütt, B. Steffen, B. Wagner, T. Weiland, S. Wipf, and H. Wolter [1992], "Solution of Maxwell's Equations," *Computer Physics Communications*, **72**, pp. 22-39.

A. Ben-Menahem and S. J. Singh [1981], *Seismic Waves and Sources*, New York, Springer.

A. D. Berlincourt, D. R. Curran, and H. Jaffe [1964], "Piezoelectric and Piezomagnetic Materials and Their Function in Transducers," in W. P. Mason (ed.), *Physical Acoustics, Principles and Methods*, **I**, Part A, New York, Academic Press, pp. 169-270.

J.-P. Berenger [1994], "A Perfectly Matched Layer for the Absorption of Electromagnetic Waves," *Journal of Computational Physics*, **114**, pp. 185-200.

M. Bihn [1998], *To the Numerical Calculation of Elastic Waves in the Time Domain*, Aachen, Shaker Verlag (in German).

M. Born and E. Wolf [1989], *Principles of Optics, Sixth Edition*, Oxford, UK, Pergamon Press.

A. Bossavit [1998], *Computational Electromagnetism, Variational Formulations, Complementary, Edge Elements*, San Diego, Academic Press.

A. Bossavit [2001], "'Generalized Finite Differences' in Computational Electromagnetics," in F. L. Teixeira (ed.), *Geometric Methods for Computational Electromagnetics*, *Progress in Electromagnetics Research (PIER)*, **32**, pp. 45-64
(see http://ceta-mac1.mit.edu/pier/pier32/02.bossavit.pdf).

C. Campbell [1998], *Surface Acoustic Wave Devices for Mobile and Wireless Communications*, San Diego, Academic Press.

H. Chen [1983], *Theory of Electromagnetic Waves*, New York, McGraw-Hill.

W. C. Chew and Q. H. Liu [1996], "Perfectly Matched Layer for Elastodynamics: A New Absorbing Boundary Condition," *Journal of Computational Acoustics*, **4**, 4, pp. 341-359.

M. Clemens [1998], *To the Numerical Calculation of Slowly Time Varying Electromagnetic Field with the Finite Integration Technique*, PhD Thesis, Darmstadt University of Technology, Darmstadt, Germany (in German).

M. Clemens, R. Schuhmann, and T. Weiland [1999], "Algebraic Properties and Conservation Laws in the Discrete Electromagnetism," *Frequenz*, **53**, pp. 219-225.

M. Clemens and T. Weiland [1999], "Numerical Algorithms for the FDiTD and FDFD Simulation of Slowly Varying Electromagnetic Fields," *International Journal of Numerical Modelling: Electronic Networks, Devices and Fields*, **12**, pp. 3-22.

M. Clemens, E. Gjonaj, P. Pinder, and T. Weiland [2000], "Numerical Simulation of Coupled Transient Thermal and Electromagnetic Fields with the Finite Integration Method," *IEEE Transactions on Magnetics*, **MAG-36**, 4, July, pp. 1448-1452.

M. Clemens and T. Weiland [2001], "Discrete Electromagnetism with the Finite Integration Technique," in F. L. Teixeira (ed.), *Geometric Methods for Computational Electromagnetics*, *Progress in Electromagnetics Research (PIER)*, **32**, pp. 65-87 (see http://ceta-mac1.mit.edu/pier/pier32/03.clemens.pdf).

M. Clemens, S. Drobny, and T. Weiland [2001], "Time Integration of Slowly-Varying Electromagnetic Field Problems Using the Finite Integration Technique," in U. van Rienen, M. Günther, and D. Hecht (eds.), *Scientific Computing in Electrical Engineering*, Berlin, Springer Verlag, pp. 63-70.

R. Courant, K. Friedrichs, and H. Lewy [1928], Über die partiellen Differenzengleichungen der mathematischen Physik," *Mathematische Annalen*, **100**, pp. 32-74.

CST [2001], Web site: http://www.cst.de.

X.-W. Dai and R. Ludwig [1990], "Numerical Simulation of Pulsed Eddy-Current Nondestructive Testing Phenomena," *IEEE Transactions on Magnetics*, **MAG-26**, 6, pp. 3089-3096.

Discrete Physics [2001], Web site: http://www.dic.univ.trieste.it/perspage/DiscretePhysics.

J. Fang [1989], *Time Domain Finite Difference Computation for Maxwell's Equations*, PhD Thesis, University of Berkeley, Berkeley.

T. Fei and K. Larner [1995], "Elimination of Numerical Dispersion in Finite-Difference Modeling and Migration by Flux-Corrected Transport," *Geophysics*, **60**, 6, pp. 1830-1842.

P. Fellinger and K. J. Langenberg [1990], "Numerical Techniques for Elastic Wave Propagation and Scattering," in S. K. Datta, J. D. Achenbach, and Y. S. Rajapakse (eds.), *Elastic Waves and Ultrasonic Nondestructive Evaluation*, Amsterdam, North-Holland, pp. 81-86.

P. Fellinger [1991], *A Method for the Numerical Solution of Elastic Wave Propagation Problems in the Time Domain by Direct Discretization of the Elastodynamic Governing Equations*, PhD Thesis, University of Kassel, Kassel, Germany (in German).

P. Fellinger and R. Marklein [1991], "EFIT – Elastodynamic Finite Integration Technique for the Modeling of the Excitation, Propagation, and Diffraction of Elastic Waves," in German Society for Non-Destructive Testing, Berlin (ed.), *Presentations of the Seminar: Models and Theories for the US Evaluation*, **23**, pp. 48-58 (in German) (available from http://www.dgzfp.de./doc/Publikationen/).

P. Fellinger, R. Marklein, K. J. Langenberg, and S. Klaholz [1995], "Numerical Modeling of Elastic Wave Propagation and Scattering with EFIT – Elastodynamic Finite Integration Technique," *Wave Motion*, **21**, pp. 47-66.

fdtd.org [2001], Web site: http://www.fdtd.org.

B. Gustafsson, H.-O. Kreiss, and J. Oliger [1995], *Time Dependent Problems and Difference Methods*, New York, John Wiley & Sons.

S. Halkjær [2000], *Elastic Wave Propagation in Anisotropic Inhomogeneous Materials*, PhD Thesis, Technical University of Denmark, Lyngby, Denmark (available from http://www.imm.dtu.dk/documents/ftp/phdliste/phd74.abstract.html).

S. Halkjær, M. P. Sørensen, and W. D. Kristensen [2000], "The Propagation of Ultrasound in an Austenitic Weld," *Ultrasonics*, **38**, 1-8, 256-261.

R. Hannemann [2001], *Modeling and Imaging of Elastodynamic Wave Fields in Inhomogeneous Anisotropic Media – An Object-Oriented Approach*, PhD Thesis, University of Kassel, Kassel, Germany (available from http://www.dissertation.de).

K.-Y. Hashimoto [2000], *Surface Acoustic Wave Devices in Telecommunications*, Berlin, Springer.

H. A. Haus and J. R. Melcher [1989], *Electromagnetic Fields and Energy*, Englewood Cliffs, NJ, Prentice Hall (online version at MIT: http://web.mit.edu/6.013_book/www/).

M. Hilgner [2001], *The Generation of Problem Matched Grids for the Calculation of Electromagnetic Fields with the Finite Integration Technique*, Aachen, Shaker Verlag (in German) (available from http://www.shaker.de).

A. T. de Hoop [1995], *Handbook of Radiation and Scattering of Waves*, London, Academic Press.

J. Kostka [1999], *Simulation and Inversion of the Propagation of Elastic Waves*, Aachen, Shaker Verlag (in German) (available from http://www.shaker.de).

K. S. Kunz and R. J. Luebbers [1993], *The Finite Difference Time Domain Method for Electromagnetics*, Boca Raton, FL, CRC Press.

L. D. Landau, E. M. Lifschitz, and L. P. Pitaevski [1984], *Electrodynamics of Continuous Media*, Oxford, Pergamon Press.

K. J. Langenberg, P. Fellinger, R. Marklein, P. Zanger, K. Mayer, and T. Kreutter [1993], "Inverse Methods and Imaging," in J. D. Achenbach (ed.), *Evaluation of Materials and Structures by Quantitative Ultrasonics*, Vienna, Springer, pp. 317-398.

K. J. Langenberg and R. Marklein [1994], "Validation of a Numerical Finite Integration Code to Solve Transient Electromagnetic, Acoustic and Elastic Wave Scattering in 2D," in *Conference Proceedings of the 10th Annual Review of Progress in Applied Computational Electromagnetics*, Monterey, pp. 180-187 (see http://aces.ee.olemiss.edu).

K. J. Langenberg, M. Brandfaß, S. Klaholz, R. Marklein, K. Mayer, A. Pitsch, and R. Schneider [1997], "Applied Inversion in Nondestructive Testing," in A. K. Louis, H. W. Engl, and W. Rundell (eds.), *Inverse Problems in Medical Imaging and Nondestructive Testing*, Vienna, Springer, pp. 93-119.

K. J. Langenberg, M. Brandfaß, R. Hannemann, Ch. Hofmann, T. Kaczorowski, J. Kostka, R. Marklein, K. Mayer, and A. Pitsch [1999], "Inverse Scattering with Acoustic, Electromagnetic, and Elastic Waves as Applied in Nondestructive Testing," in A. Wirgin (ed.), *Wavefield Inversion*, Vienna, Springer, pp. 59-118.

K. J. Langenberg, R. Hannemann, T. Kaczorowski, R. Marklein, B. Koehler, C. Schurig, and F. Walte [2000], "Application of Modeling Techniques For Ultrasonic Austenitic Weld Inspection," *NDT & E International*, **33**, pp. 465-480.

K. J. Langenberg, R. Marklein, and K. Mayer [2002], "Applications to Nondestructive Testing with Ultrasound," in E. R. Pike and P. C. Sabatier (eds.), *Scattering: Scattering and Inverse Scattering in Pure and Applied Science*, **1**, London, Academic Press, pp. 594-617.

R. Lerch [1990], "Simulation of Piezoelectric Devices by Two- and Three-Dimensional Finite Elements," *IEEE Transactions on Ultrasonics, Ferroelectrics, and Frequency Control*, **37**, 2, pp. 233-247.

R. Ludwig and X.-W. Dai [1991], "Numerical Simulation of Electromagnetic Acoustic Transducer in the Time Domain," *J. Appl. Phys*, **69**, pp. 89-98.

R. Madariaga [1976], "Dynamic of an Expanding Circular Fault," *Bulletin Seismological Society of America*, **66**, 3, pp. 639-666.

R. Marklein and P. Fellinger [1991], "Mathematic-Numerical Modeling of Propagation and Diffraction of Acoustic Waves," in German Society for Non-Destructive Testing, Berlin (ed.), *Presentations of the Seminar: Models and Theories for the US Evaluation*, **23**, pp. 58-68 (in German) (see http://www.dgzfp.de./doc/Publikationen/).

R. Marklein, R. Bärmann, and K. J. Langenberg [1995], "The Ultrasonic Modeling Code EFIT as Applied to Inhomogeneous Dissipative Isotropic and Anisotropic Media," in D. O. Thomson and D. E. Chimenti (eds.), *Review of Progress in Quantitative Nondestructive Evaluation*, **14**, New York, Plenum Press, pp. 251-258.

R. Marklein, K. J. Langenberg, and T. Kaczorowski [1996], "Electromagnetic and Elastodynamic Point Source Excitation of Unbounded Homogeneous Anisotropic Media," *Radio Science*, **31**, 6, pp. 1919-1930.

R. Marklein, K. J. Langenberg, K. Mayer, S. Klaholz, and J. Kostka [1997], "Computation and Visualization of Acoustic and Elastic Waves in Nondestructive Testing (NDT)," in *Proceedings of the 15th IMACS World Congress on Scientific Computation, Modeling and Applied Mathematics*, Berlin, Germany, Wissenschaft und Technik Verlag, pp. 507-512.

R. Marklein and O. Glitza [1997], "The Piezoelectric Finite Integration Technique (PFIT) – A Novel Numerical Method to Model Piezoelectric Transducers/Sensors and Ultrasonic Wave

Phenomena in the Time Domain," in *Proceedings of the International Symposium on Electromagnetic Theory*," Thessaloniki, **2**, pp. 754-756 (available from http://www.ursi.org).

R. Marklein [1997], *Numerical Methods for the Modeling of Acoustic, Electromagnetic, Elastic and Piezoelectric Wave Propagation Problems in the Time Domain Based on the Finite Integration Technique*, Aachen, Shaker Verlag (in German) (available from http://www.shaker.de).

R. Marklein, O. Glitza, T. Kaczorowski, and K. J. Langenberg [1998], "Numerical Time Domain Modeling of Piezoelectric Transducers/Sensors and Ultrasonic Wave Phenomena with the Piezoelectric Finite Integration Technique (PFIT)," in D. O. Thomson and D. E. Chimenti (eds.), *Review of Progress in Quantitative Nondestructive Evaluation*, **18**, New York, Plenum Press, pp. 1053-1069.

R. Marklein and K. J. Langenberg [1998], "Numerical Modeling of Acoustic, Elastic, and Piezoelectric Wave Propagation and Scattering with AFIT, EFIT, and PFIT," in *Proceedings of the 2nd International Conference on Computer Methods and Inverse Problems in Nondestructive Testing and Diagnostics*, Minsk, Belarus, **51**, pp. 157-172 (available from http://www.dgzfp.de./ doc/Publikationen/).

R. Marklein, K. J. Langenberg, G. Hübschen, and H. Willems [1999], "Numerical Time Domain Modeling of the Ultrasonic NDT with Electromagnetic Acoustic and Piezoelectric Transducers," in D. O. Thomson and D. E. Chimenti (eds.), *Review of Progress in Quantitative Nondestructive Evaluation*, **19**, New York, Plenum Press, pp. 1001-1008.

R. Marklein [2000a], "Unified Numerical Calculation of Acoustic, Electromagnetic, Elastodynamic, and Piezoelectric Waves," *Kleinheubacher Berichte*, **43**, pp. 399-410 (in German) (available from T-Nova Deutsche Telekom Innovationsgesellschaft mbH, Technologiezentrum, Abt. E45, D-64307 Darmstadt, Germany).

R. Marklein [2000b], "Unified Numerical Time-Domain Modeling of Acoustic, Electromagnetic, Elastic, Piezoelectric, and Electromagnetic-Ultrasonic Waves," in *Proceedings of the 16th IMACS World Congress on Scientific Computation, Modeling and Applied Mathematics*, CD-ROM (available from http://www.cs.rutgers.edu/~imacs and http://www.imamod.ru/jour/conf/IMACS_2000/CP/414-6.pdf).

M. Marrone [2001], "Computational Aspects of Cell Method in Electrodynamics," in F. L. Teixeira (ed.), *Geometric Methods for Computational Electromagnetics*, *Progress in Electromagnetics Research (PIER)*, **32**, pp. 317-356 (see http://ceta-mac1.mit.edu/pier/pier32/13.marrone.pdf).

C. Mattiussi [1997], "An Analysis of Finite Volume, Finite Element, and Finite Difference Methods Using Some Concepts from Algebraic Topology," *Journal of Computational Physics*, **133**, pp. 289-309.

C. Mattiussi [2000], "The Finite Volume, Finite Element, and Finite Difference Methods as Numerical Methods for Physical Field Problems," in P. Hawkes (ed.), *Advances in Imaging and Electron Physics*, **113**, pp. 1-146.

C. Mattiussi [2001], "The Geometry of Time-Stepping," in F. L. Teixeira (ed.), *Geometric Methods for Computational Electromagnetics*, *Progress in Electromagnetics Research (PIER)*, **32**, pp. 123-149 (see http://ceta-mac1.mit.edu/pier/pier32/05.mattiussi.pdf).

J. Miklowitz [1980], *The Theory of Elastic Wave Guides, Second Edition*, Amsterdam, North-Holland.

M. A. Morgan (ed.) [1989], *Finite Element and Finite Difference Methods in Electromagnetic Scattering*, *Progress in Electromagnetics Research (PIER)*, **2**, New York, Elsevier (see http://www.emwave.com/pierbook.htm).

D. F. Nelson [1979], *Electric, Optic, and Acoustic Interactions in Dielectrics*, New York, John Wiley & Sons.

A. Peiffer, B. Köhler, and S. Petzold [1997], "The Acoustic Finite Integration Technique for Waves of Cylindrical Geometry (CAFIT)," *Journal of Acoustical Society of America*, **102**, 2, pp. 697-706.

P. Pinder [1998], *The Numerical Calculation of Coupled Electromagnetic and Thermal Fields*, PhD Thesis, Darmstadt University of Technology, Darmstadt, Germany (in German).

R. D. Richtmyer and K. W. Morton [1967], *Difference Methods for Initial Value Problems, Second Edition*, New York, John Wiley & Sons.

M. J. Roberts [1991], *Numerical Modeling of Piezoelectric Transducer Arrays for Medical Imaging Systems*, PhD Thesis, Worcester Polytechnic Institute (WPI), Worcester, MA, USA.

D. Royer and E. Dieulesaint [2000a], *Elastic Waves in Solids I: Free and Guided Propagation*, Berlin, Springer.

D. Royer and E. Dieulesaint [2000b], *Elastic Waves in Solids II: Generation, Acousto-Optic Interaction, Applications*, Berlin, Springer.

E. H. Saenger, N. Gold, and S.A. Shapiro [2000], "Modeling the Propagation of Elastic Waves Using a Modified Finite-Difference Grid," *Wave Motion*, **31**, pp. 77-92.

C. T. Schröder and W. R. Scott [2000], "A Finite-Difference Model to Study the Elastic-Wave Interaction with Buried Land Mines," *IEEE Transactions on Geoscience and Remote Sensing*, **38**, 4, pp. 1505-1512.

F. Schubert, A. Peiffer, B. Köhler, and T. Sanderson [1998], "The Elastodynamic Finite Integration Technique for Waves in Cylindrical Geometries," *Journal of Acoustical Society of America*, **104**, 5, pp. 2604-2614.

F. Schubert [2000], "*Propagation Characteristics of Ultrasonic Waves in Concrete and Resulting Aspects for Their Non-Destructive Testing*," PhD Thesis, Dresden University of Technology, Dresden, Germany (in German).

F. Schubert, B. Köhler, and A. Peiffer [2001], "Time Domain Modeling of Axisymmetric Wave Propagation in Isotropic Elastic Media with CEFIT-Cylindrical Elastodynamic Finite Integration Technique," *Journal of Computational Acoustics*, **9**, 3, pp. 1127-1146.

F. Schubert and B. Köhler [2001], "Modeling of Linear and Nonlinear Elastic Wave Propagation Using Finite Integration Techniques in Cartesian and Curvilinear Coordinates," in *Proceedings on Elastic Waves in Nondestructive Testing*, Euromech 419, Prague, Czech Republic (to appear).

S. Schuhmacher [1997], *Consistent Emitter-Receiver-Modeling of Piezoelectric Transducers Applied in Non-Destructive Testing with Ultrasound Based on Auld's Reciprocity Theorem*, PhD Thesis, University of Saarbrücken, Saarbrücken, Germany (in German).

R. Schuhmann [1999], *The Non-Orthogonal Finite Integration Technique for the Simulation of Electromagnetic Fields*, PhD Thesis, Darmstadt University of Technology, Darmstadt, Germany (in German).

R. Schuhmann and T. Weiland [2001], "Conservation of Discrete Energy and Related Laws in the Finite Integration Technique," in F. L. Teixeira (ed.), *Geometric Methods for Computational Electromagnetics*, *Progress in Electromagnetics Research (PIER)*, **32**, pp. 301-316 (see http://ceta-mac1.mit.edu/pier/pier32/12.shumann.pdf).

W. R. Scott, J. S. Martin, and G. D. Larson [2001], "Experimental Model for a Seismic Landmine Detection System," *IEEE Transactions on Geoscience and Remote Sensing*, **39**, 6, pp. 1155-1164.

H. Shirai and L. B. Felsen [1987], "Rays, Modes and Beams for Plane Wave Coupling Into a Wide Open-Ended Parallel-Plane Waveguide," *Wave Motion*, **9**, pp. 301-317.

J. C. Strikwerda [1989], *Finite Difference Schemes and Partial Differential Equations*, Pacific Grove, CA, Mathematics Series, Wadsworth & Brooks/Cole.

D. M. Sullivan [2000], *Electromagnetic Simulation Using the FDTD Method*, Piscataway, NJ, IEEE Press.

C.-T. Tai [1997], *Generalized Vector and Dyadic Analysis, Second Edition*, New York, IEEE Press.

A. Taflove [1998], *Advances in Computational Electrodynamics: The Finite-Difference Time-Domain Method*, Boston, Artech House.

A. Taflove and S. Hagness [2000], *Computational Electrodynamics: The Finite-Difference Time-Domain Method, Second Edition*, Boston, Artech House.

F. L. Teixeira and W. C. Chew [1999a], "Lattice Electromagnetic Theory from a Topological Viewpoint," *Journal of Mathematical Physics*, **40**, 1, pp. 169-187.

F. L. Teixeira and W. C. Chew [1999b], "Differential Forms, Metrics, and the Reflectionless Absorption of Electromagnetic Waves," *Journal of Electromagnetic Waves and Applications*, **13**, 5, pp. 665-686.

F. L. Teixeira (ed.) [2001], *Geometric Methods for Computational Electromagnetics*, *Progress in Electromagnetics Research (PIER)*, **32** (see http://ceta-mac1.mit.edu/pier/pier32/pier32.html).

R. B. Thompson [1993], "Electromagnetic-Acoustic Transducers (EMATs)," in J. D. Achenbach (ed.), *Evaluation of Materials and Structures by Quantitative Ultrasonics*, Wien, Springer Verlag, pp. 71-104.

P. Thoma [1997], *To the Numerical Solution of Maxwell's Equations in the Time Domain*, PhD Thesis, Darmstadt University of Technology, Darmstadt, Germany (in German).

E. Tonti [2001a], "A Direct Discrete Formulation of Field Laws: The Cell Method," *CMES-Computer Modeling in Engineering and Sciences*, **2**, 2, pp. 237-258 (see http://www.dic.univ.trieste.it/perspage/DiscretePhysics/).

E. Tonti [2001b], "Finite Formulation of the Electromagnetic Field," in F. L. Teixeira (ed.), *Geometric Methods for Computational Electromagnetics*, *Progress in Electromagnetics Research (PIER)*, **32**, pp. 1-44 (see http://ceta-mac1.mit.edu/pier/pier32/01.tonti.pdf).

U. van Rienen [2001a], *Numerical Methods in Computational Electrodynamics; Linear Systems in Practical Applications*, Berlin, Springer.

U. van Rienen [2001b], "Frequency Domain Analysis of Waveguides and Resonators with FIT on Non-Orthogonal Triangular Grids," in F. L. Teixeira (ed.), *Geometric Methods for Computational Electromagnetics*, *Progress in Electromagnetics Research (PIER)*, **32**, pp. 357-381 (see http://ceta-mac1.mit.edu/pier/pier32/14.vanrienen.pdf).

J. Virieux [1984], "SH Wave Propagation in Heterogeneous Media: Velocity-Stress Finite-Difference Method," *Geophysics*, **49**, 11, pp. 1933-1957.

J. Virieux [1986], "P-SV Wave Propagation in Heterogeneous Media: Velocity-Stress Finite-Difference Method," *Geophysics*, **51**, 4, pp. 889-901.

J. L. Volakis, A. Chatterjee, and L. C. Kempel [1998], *Finite Element Method for Electromagnetics, Antennas, Microwave Circuits, and Scattering Applications*, Piscataway, NJ, IEEE Press.

T. Weiland [1977], "A Discretization Method for the Solution of Maxwell's Equations for Six-Component Fields," *Electron. Commun. (AEÜ)*, **31**, 3, pp. 116-120 (see http://www.tu-darmstadt.de/fb/et/temf/).

T. Weiland [1986], "The Discretization of Maxwell's Equations," *Physikalische Blätter*, **42**, 7, pp. 191-201 (in German).

T. Weiland [1996], "Time Domain Electromagnetic Field Computation with Finite Difference Methods," *International Journal of Numerical Modelling: Electronic Networks, Devices and Fields*, **3**, pp. 295-319.

H. Wolter [1995], *Calculation of Acoustic Waves and Resonators with the FIT Method*, PhD Thesis, Darmstadt University of Technology, Darmstadt (in German).

K. S. Yee [1966], "Numerical Solution of Initial Boundary Value Problems Involving Maxwell's Equations in Isotropic Media," *IEEE Transactions on Antennas and Propagation*, **AP-14**, pp. 302-307.

K. S. Yee, J. S. Chen, and A. H. Chang [1992], "Conformal Finite-Difference Time-Domain (FDTD) with Overlapping Grids," *IEEE Transactions on Antennas and Propagation*, **AP-40**, 9, pp. 1068-1075.

K. S. Yee and J. S. Chen [1997a], "The Finite-Difference Time-Domain (FDTD) and the Finite-Volume Time-Domain (FVTD) Methods in Solving Maxwell's Equations," *IEEE Transactions on Antennas and Propagation*, **AP-45**, 3, pp. 354-363.

K. S. Yee and J. S. Chen [1997b], "Impedance Boundary Condition Simulation in the FDTD/FVTD Hybrid," *IEEE Transactions on Antennas and Propagation*, **AP-45**, 6, pp. 921-925.

X. Yuan, D. Borup, M. Berggeren, R. Eidens, and S. A. Johnson [1997], "Formulation and Validation of Berenger's PML Absorbing Boundary for the FDTD Simulation of Acoustic Scattering," *IEEE Transactions on Ultrasonics, Ferroelectrics, and Frequency Control*, **44**, 4, pp. 816-822.